College of Natural and Computational Science

Department of Chemistry

MSc. Thesis On:

Green Synthesis of Iron Oxide Nanoparticles Using *Adhatoda schimperiana (Simiza)* Leaf aqueous Extract for Methylene Blue Dyes Degradation and Anti-Bacterial Activity.

The Thesis Submitted to Department of Chemistry in partial fulfillment of the requirements for the degree Master of Science in Chemistry (Analytical).

By: Desiew Mekuanint Getahun

Advisor: Asamene Embiale (PhD)

January, 2025

Woldia, Ethiopia

Woldia University

College of Natural and Computational Sciences

Department of Chemistry

MSc. Thesis Research On:

"Green Synthesis of Iron Oxide Nanoparticles Using *Adhatoda schimperiana* Leaf aqueous Extract for Methylene Blue Dyes Degradation and Anti-Bacterial Activity Application".

The Thesis Submitted to Department of Chemistry Woldia University in partial fulfillment of the requirements for the degree Master of Science in Chemistry (Analytical).

By: Desiew Mekuanint Getahun

Advisor: Asamene Embiale (PhD)

January, 2025

Woldia, Ethiopia

Woldia University

College of Natural and Computational Sciences

Department of Chemistry

Thesis Approval Sheet

I/we, the advisors of the thesis entitled "**Green Synthesis of Iron Oxide Nanoparticles Using *Adhatoda schimperiana ('Simiza')* Leaf aqueous Extract for Methylene Blue Dyes Degradation and Anti-Bacterial Activity Application**" and developed by Desiew Mekuanint Getahun, him by certify that the recommendation and suggestions made by the board of examiners are appropriately incorporated into the final version of the thesis.

Advisor	Signature	Date

Approval of Board of Reviewers I/we, the undersigned, members of the board of Examiners this thesis to be prepared by Desiew Mekuanint Getahun, entitled: In **"Green Synthesis of Iron Oxide Nanoparticles Using *Adhatoda schimperiana ('Simiza')* aqueous Leaf Extract for Methylene Blue Dyes Degradation and Anti-Bacterial Activity Application"** and submitted in partial fulfillment of the requirements for the degree of Master of Science in Chemistry (Analytical Chemistry) with the regulations of the University and meets the accepted standards with respect to originality and quality.

Approved and signed by the examining committee:

Chairperson	Signature	Date
Internal Examiner	Signature	Date

External Examiner	Signature	Date

Final approval and acceptance of the thesis is contingent upon submission of its final copy to the Office of Postgraduate Studies (OPGS) through the Department Graduate Council (DGC) and College Graduate Committee (SGC).

Department Head	Signature	Date
Collage Dean	Signature	Date
Office of Postgraduate Studies, Dean	Signature	Date

Declaration

The under signed, declare that the thesis entitled " **Green Synthesis of Iron Oxide Nanoparticles Using *Adhatoda schimperiana ('Simiza')* Leaf aqueous Extract for Methylene Blue Dyes Degradation and Anti-Bacterial Activity Application"** has not been done in substance for the award of any degree in any other university. All sources of the materials used in this thesis have appropriately have been acknowledged.

Desiew Mekuanint Getahun	_____	_____
Name of student	Signature	Date

Acknowledgment

First of all, I would like to thank the almighty God and St. Mary for being source of my Capability and strength to reach this period of thesis and throughout my life.

I would like to express my deepest gratitude and respect to my research advisor Asamene Embiale (PhD) for his patience, understanding, guidance, constructive comments and suggestions throughout my thesis work.

I would like to thank my staff member in Department of Chemistry for give this chance and help me by fill up any gap throughout my work as well as I am extremely grateful to my best friends Adno Asmare, Habtam Dems and wondefraw Teshome with a deep sense of gratitude that helped me in facilitating conditions and resources throughout my study and lastly I am thankful to the Woldia University for providing the sponsorship.

Table of contents

List of figures

List of tables

List of abbreviations

A. Schimperiana-NPs	*Adhatoda schimperiana* nano particles.
A.Schimperiana	*Adhatoda schimperiana*.
BET	*Brunauer-Emmett-Teller*
E. coli	*Escherichia coli*.
FTIRS	Fourier transforms infra-red spectroscopy.
IONPs	Iron oxide nano particles.
MB	Methylene blue.
MDR	Multi-drug resistances.
NPs	Nano particles
RPM	Rotation per minute
S.aureus	*Staphylococcus aureus*
S.Pyogenes	*Streptococcus pyogenes*
TGA	Thermo gravimetric analysis
UV-Vis	UV-Visible light spectroscopy
XRD	X-Ray-diffraction

Abstract

Among various metal and metal oxide nanoparticles, iron-oxide nanoparticles have been more widely used for the degradation of harmful organic dyes and the inhibition of microbial growth. In this study, Fe_2O_3 nanoparticles were prepared from *Adhatoda schimperiana* leaf aqueous extract and used to degrade Methylene Blue dye and inhibit microbes. UV-visible spectroscopy, TGA, FTIR, XRD and BET were employed to characterize the synthesized nanoparticles. The influence of pH, adsorbent dosage, contact time, and adsorbate concentration on methylene blue dye removal by iron oxide nanoparticles was investigated. The UV-Vis absorbance shift from 416 nm to 397 nm (by 19 nm) suggested the synthesize of iron oxide nanoparticles. The XRD spectrum of Fe_2O_3 nanoparticles revealed a remarkably clean and crystalline structure with an average particle diameter of 14.31 nm. The surface area of uncalcineate and calcinated Fe_2O_3 was 276.3 m^2/g and 286.8 m^2/g, respectively, according to BET analysis. The FTIR spectra confirmed the signature bands for Fe-O (574.1 cm^{-1}) and organic moieties stretching vibrations. The point of zero charge iron oxide nanoparticles was 8.27, with a pH of 9. The thermal stability was determined by TGA, which revealed a 3.412% weight loss. Fe_2O_3 nanoparticles were reported to have a photo catalytic degradation rate of 97.082% for methylene blue. Using the well diffusion method, it was shown that synthesized iron oxide nanoparticles and plant extract exhibit antibacterial activity against gram-positive (*Salmonella, Staphylococcus aureus*,) and gram-negative (*Escherichia coli*) with the inhibition zone were 13.7 mm, 16 mm and 18 mm respectively. This green synthetic approach has been discovered to be easy ecologically friendly, and promising for usage in a range of applications, including pollutant removal from water bodies and antibacterial testing.

Keywords

Anti-bacterial activity, Adhatoda schimperiana, Green synthesis, Iron oxide nano particles, Methylene blue dyes degradation.

1. Introduction

1.1 Back ground of the study

The quality of nature's gift of water has degraded as a result of industrialization and other man-made activities, excessive chemical usage, and inappropriate product disposal [1]. Among the pollutants discharges from the companies such as azo, fiber-reactive, basic, acid, and dispersion dyes as pollutants [2]. A wide range of industries, including food, cosmetics, textiles, paint, printing, carpet, and paper, use dyes as colorants. Due to inappropriate handling, these colors have seriously damaged the environment, particularly water bodies, and exposed humans which can cause for harmful diseases like cancer, liver, kidney, brain, skin disorders, allergies, and mutations as well as aquatic life's ability to photosynthesis is impacted by light penetration that is blocked by dyes in the water system [3] . Thus, such types of problems can be overcome using different types of nanoparticles, particularly metal oxide nanoparticles [4].

On the other hand, antimicrobial resistance (AMR) is one of the worlds' challenges that require immediate solution. AMR refers to a microorganism's capacity to resist the effects of a medication that used to be able to cure the bacteria. This is accomplished through four mechanisms: (1) drug uptake limitation; (2) drug target modification; (3) drug inactivation; and (4) active drug efflux [5]. Safe and affordable plant extract-mediated nanoparticles have been showing promising results in resolving AMR. Among the several methods of synthesis of nanoparticles using a variety of techniques such as chemical, physical, and biological. From this method the biological molecules are assembled undergo highly control to make them appropriate for the production of metal nanoparticles, which have been proven to be dependable, accessible, nontoxic, and environmentally friendly. An environmentally friendly synthetic method for the synthesis of nanoparticles is generating interest globally in a biological method that free from the use of dangerous chemicals as by products. Many biological techniques for synthesis nanoparticles have been reported so far, employing microorganisms like bacteria, fungi, and plants [6, 7]. Of them, plants offer a superior substrate for the synthesis of nanoparticles. This is due to the fact that the synthesis of nanoparticles using plant extracts has several advantages over other methods, such as being inexpensive, effective, and environmentally friendly. Additionally, the plants are widely available, easily handled, and serve as a source of multiple metabolites by

the process. Nanotechnology's primary interests are the production of nanoparticles with different sizes, shapes, chemical compositions, control discrepancies, and possible applications for human benefit [8, 9]. The size, shape, texture, and chemical composition of these nanoparticles will all affect their potential. Due to their small size and high surface-to-volume ratio, these particles find extensive applications in biotechnology, microbiology, electronics, optics, mechanics, environmental remediation, medicine, and food technology [10]. Both the specific surface area and the proportion of surface atoms of metal nanoparticles are large since nanoparticles' unique physico-chemical properties such as adsorption, catalytic activity, optical, electronic, antibacterial properties, photo catalytic, and magnetic properties are gaining scientists' attention due to their novel methods of synthesis [11, 12].

Metal oxide nanoparticles, like iron oxide nanoparticles, are widely used as catalysts, solar power converters, environmental protectors, sensors, biomedical applications, tissue repair, magnetic storage mediums, reactive oxygen species-induced oxidative stress, and drug delivery. Additionally iron oxide nanoparticles are utilized as an adsorbent in wastewater treatment and as nano medicines because of their exceptional ability to remove a variety of water pollutants and threat for antibacterial Activity [13]. Hence, presently several researchers have been reported on the synthesis of iron oxide nanoparticles using medicinal plants such as [14], *Eucalyptus* leaf extract [15], *Carica papaya* plant leaf extract [16], *Siceraria* leaf extract [17] ,*Solanum nigrum* leaf extract [18], *Guava* leaf extract as insect repellent [19] , *Citrus* (leome) leaf extract [20], *Coriandrum sativum* leaf extract [21]. Similarly to other medicinal plants *Adhatoda schimperiana* plant has given a priority by the field of biomedical, pharmaceutical and biological industries for different applications, more importantly for nanoparticle synthesis. This might be due the presence of phytochemicals including: polyphenols, tannins, alkaloids, flavonoids, saponins etc…. These phytochemicals are responsible for reducing the metal ions and then stabilizing during metal nanoparticle synthesis. Although *Adhatoda schimperiana* leaf extract used for the synthesis of CuO nanoparticles [22]. No report has been available for the preparation of iron oxide nanoparticles using *Adhatoda schimperiana* leaf extract. Therefore, *Adhatoda schimperiana* has been selected for this study to synthesis of iron oxide nanoparticle for the application degradation of methyl bule dyes and anti-bacterial activity.

1.2 Statement of the problem

Adhatoda schimperiana is used as traditional medicine in rural area of Ethiopia. It is used as traditional medicine against malaria wounds, gonorrhea's rabies and other skin diseases ,wear as inadequate awareness among the public regarding to the appropriate dosage of plant medicines[23].The discovery that is still unexplained multi-drug-resistant (MDR) bacterial strains and that organic dye (MB) contamination of water is increasing made it clear that this is a significant public health concern. To address this issue, the new medications needed for the elimination of MB dye that are efficient, widely applicable, and economically feasible should be developed[24]. *So, Adhatoda schimperiana* produces a series of polyphenols, tannins, saponins and alkaloids that possess very potent and useful biological properties including antibacterial, antifungal and insecticidal properties. The bioactivities of these plants can be enhanced more when it is supported with metal/metal oxide NPs, Surface reaction phenomenon of these biosynthesized particles and high surface area to volume ratio of particles generate a tendency to interact and scavenge the free radicals. On the other hand, metal/metal oxide nanoparticles play a great role in the removal of toxic pollutants to remediate a safe environment; however, the physical and chemical methods of synthesis of metal oxide NPs are expensive and not eco-friendly [25]. Therefore, green based synthesis of nanoparticles using plant-based material is the most widely used techniques to overcome shortcoming of chemical-based synthesis of nanoparticles. Many literature reports that the research in the field of green synthesis has been mainly focusing on Ag, Cu, Au Zn, NiO, CuO and ZnO NPs. Moreover, although iron oxide nanoparticles have many applications such as to remove toxic dyes to save environmental, health problems and for antimicrobial activity, there have been very few reports on the green synthesis of iron oxide nanoparticles. As far as I know, no one has reported IONPs using *Adhatoda schimperiana* leaf extract. Hence, this research was synthesized more iron oxide nano particles (IONPs) to be cheaply available so as to be used in different fields of applications [26, 27]. Thus, for green synthesis of IONPs using more local and easily available plants are highly recommended that *Adhatoda schimperiana* ("Simiza") was implemented for this study for antibacterial activity and degradation of methyl blue dyes.

1.3 Objectives of the study

1.3.1 General objective

The main objective of this study was to synthesize and characterize iron oxide nano particles using aqueous leaf extract of *Adhatoda schimperiana* for degradation of methyl blue dye and antibacterial activity test.

1.3.2 Specific objectives

The specific objectives of this study were able to:

- To check the qualitative test of phytochemicals in *Adhatoda schimperiana* leaf extract.
- To synthesize iron oxide nano particle using aqueous leaf extract of *Adhatoda schimperiana*.
- To characterize the synthesized IONPs using UV-Vis, TGA, FTIR, XRD and BET.
- To evaluate photo catalytic activity of the synthesis IONPs using methylene blue dye.
- To evaluate the anti-bacterial activities of the synthesized IONPs against Gram-positive and Gram-negative bacteria.

1.4 The Significance of the study

Green synthesis of nanoparticle has been shown to be a superior synthesis method, because of its better manipulation, stability, and slower kinetics. Since they offer solutions for various environmental and health problems, creating nanoparticles with the appropriate size and makeup is of great interest [28]. As a result, the produced iron oxide nanoparticles utilizing *Adhatoda Schimperiana* leaf extract may have the following importance:

- The synthesized nanoparticles may be used to build medicine in the future.
- Enhance knowledge of IONP and their applications.
- The newly synthesized IONP could reduce environmental pollutants and health problems.
- The freshly synthesized IONP were serving as a basis line for future study development by other researchers.

2. Literature review

2.1 Nano materials

A material with a nanoscale dimension of 1–100 nm is called a nanoparticle. The Greek word from which the word "nanometer" is derived means "dwarf" or "extremely small." Three to five atoms arranged in a row are represented by one nanometer. A nanoscale particle's diameter is around five orders of magnitude smaller than that of a human hair. The optical, magnetic, electrical, and other physical and chemical characteristics of nanoparticles are distinct from those of molecules and bulk solid states (Metals, ceramics, polymers, and composite materials are examples of nano materials) [29, 30]. They offer a great deal of potential for usage in nanotechnology, electronics, medicine, and other domains due to their unique physical and chemical characteristics. Silica, fullerene, carbon nanotubes, silver nano, and photo catalysts are a few examples. A number of electrical and optical systems' processing, storing, and displaying components are being enhanced via nanotechnology [31, 32]. One-dimensional (like surface films), two-dimensional (like strands or fibers), or three-dimensional (like particles) nano materials are all possible. They have spherical, tubular, and irregular shapes and can be found in solitary, fused, aggregated, or agglomerated forms [31]. A collection of techniques for working with matter at a small scale to produce nanoscale objects for real-world uses is known as nanotechnology. Therefore, nanomaterial’s solid materials with distinctive properties related to their scale are the cornerstones of nano science and nanotechnology [33]. Nanotechnology is a promising science with wide applications from cosmetics, food products, clothing, and household appliances to fuel catalysts, disease treatment, and renewable energies. It is also being applied to a variety of industrial and purification processes, including construction materials, nano machining of nanowires, nano rods, grapheme, water filtration, wastewater treatment, energy storage, automotive parts, thin-film electronics, coatings, and anti-bacteria [34, 35].

2.1.1 Types of nano particles

In general, nanoparticles can be divided into two categories: inorganic nanoparticles, which are made of metal or metal oxides (such as Ag, Fe_2O_3, TiO_2, CuO, and ZnO nanoparticles), which have been investigated as possible tools for medical imaging, disease treatment, and adsorption

activity, and organic nanoparticles, which include due to their size features and advantages over available chemical imaging drug agents and drugs. Inorganic nanoparticles have been widely used for cellular delivery due to their various advantages, such as their wide availability, rich functionality, high compatibility, and ability to provide drugs with controlled release and precision [36].

2.1.2 Metal oxide nanoparticles

For a number of basic scientific and technical reasons, as well as to get access to new classes of functional materials with unique properties and uses, nano-structured metal oxides have been the subject of much research. The production of nano-sized crystalline metal oxides has garnered more attention in recent years due to their high surface areas, peculiar adsorptive qualities, surface defects, and nanoscale conductivity, diffusivity, ionic structure, freezing, melting, and color [37].

2.1.3 Iron oxide nano particle

Iron (III) oxide is an inorganic compound with the formula Fe_2O_3. The other two forms of iron oxides are iron (II) oxide (FeO), which is rare, and iron (II, III) oxide (Fe_3O_4), which occurs naturally as the mineral magnetite. Hematite, or Fe_2O_3, is the principal source of iron for the steel industry. Fe_2O_3 is paramagnetic, reddish brown, and easily dissolved by acids. Rust is comparable to iron (III) oxide in composition and properties; therefore, it can be useful to refer to it as such [38, 39].

2.2 Techniques of synthesis of iron oxide nano particles

Principally there are two approaches used to synthesize NPs including the top-down approach and the bottom-up approach (Figure 1).

I. Top-down approach to NPs synthesis: This method uses a succession of synthetic technologies to synthesis NPs by removing certain components from a bulk material substrate. Pieces can be removed from bulk materials via chemical, electrochemical, or mechanical techniques. The bulk substrate material and targeted NP size decide the technique to be used. This method, however, does not provide perfect control over particle size [40].

II. **Bottom-up approach for NPs synthesis**: involves stacking components on top of a base substrate to construct complex systems while maintaining control over the chemical structure. [41].

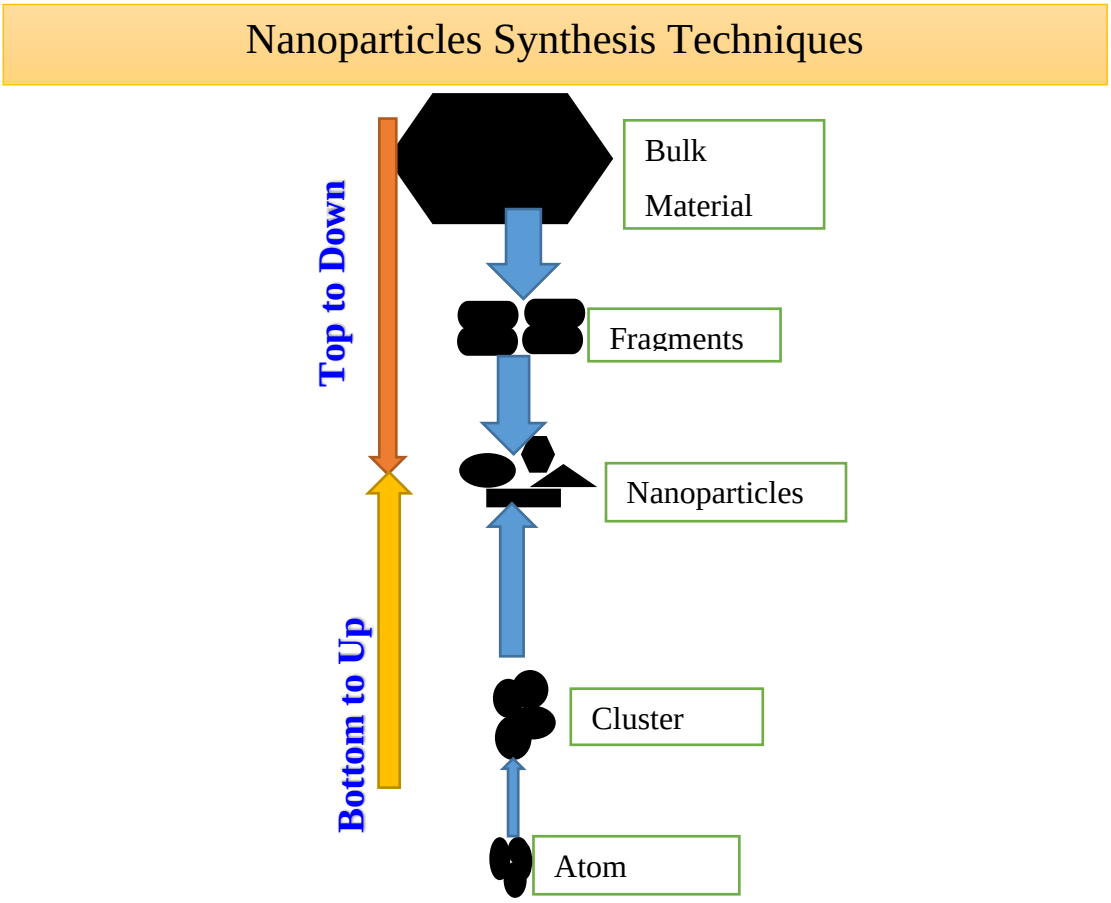

Figure 1: The schematic representation of the top-down and bottom-up approaches for production of metal oxide nano structures [42].

2.3 Synthesis methods of iron oxide nanoparticles

There are three main fabrication methods for nanoscale entities: physical, chemical, and green synthesis techniques. The physical synthesis process is mostly determined by the instruments used in the experiment. Nano materials are produced using processes such as arc discharge, ball milling, and electron beam lithography. [43]. Chemical production of nanoparticles requires chemicals, reducing and capping agents, as well as suitable temperature and pressure conditions. Electrochemical, micro emulsion and ozonation are some examples of chemical synthesis methods. The biological method of synthesis is environmentally friendly and known as "green

synthesis" since it is non-toxic, saves reagents, and does not affect living creatures. Figure 2 depicts multiple nanoparticle synthesis processes [44].

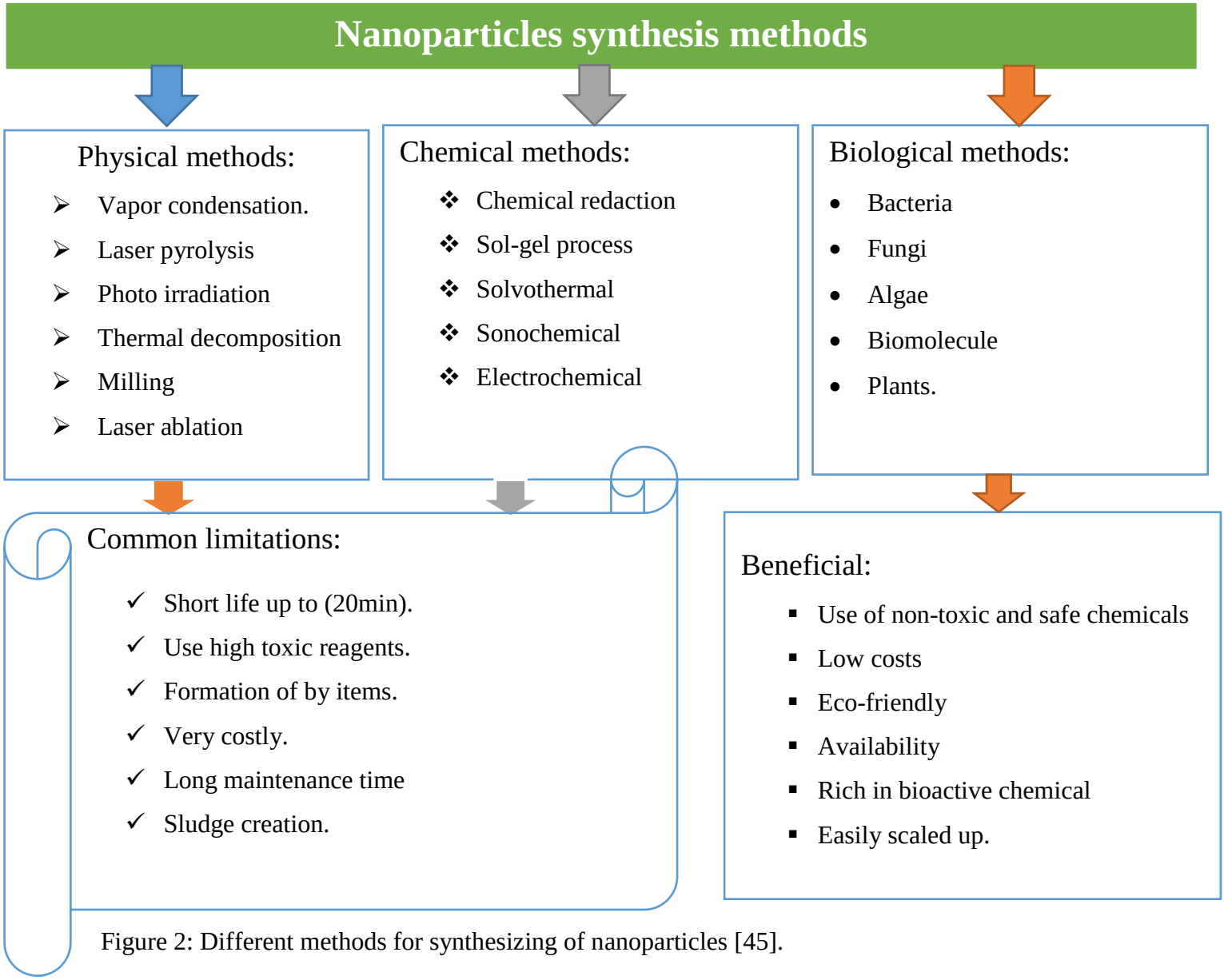

Figure 2: Different methods for synthesizing of nanoparticles [45].

2.3.1 Physical methods

Physical procedures employed include plasma arcing, ball milling, thermal evaporation, spray pyrolysis, ultrathin films, pulsed laser desorption, lithographic techniques, sputter deposition, layer-by-layer growth, molecular beam epistaxis, and diffusion flame synthesis of nanoparticles [46].

2.3.2 Chemical methods

Chemical procedures include precipitation, oxidation, or reduction, the creation of an insoluble gas followed by tripping, and other chemical reactions that require the interchanging or sharing of electrons between atoms [46].

2.3.3 Green methods

In the nanoparticle production process, green synthesis is utilized to produce environmentally beneficial materials such as bacteria, fungi, and plants. Green synthesis focuses on producing metal and metal oxide nanoparticles [47]. The development of green syntheses over chemical and physical methods is environment-friendly, cost-effective, and simply scaled up for large-scale syntheses of nanoparticles in comparison to bacteria/fungi or plant-mediated synthesis; there was no need to use high temperature, pressure, energy, and toxic chemicals [6, 48].The use of green methods.

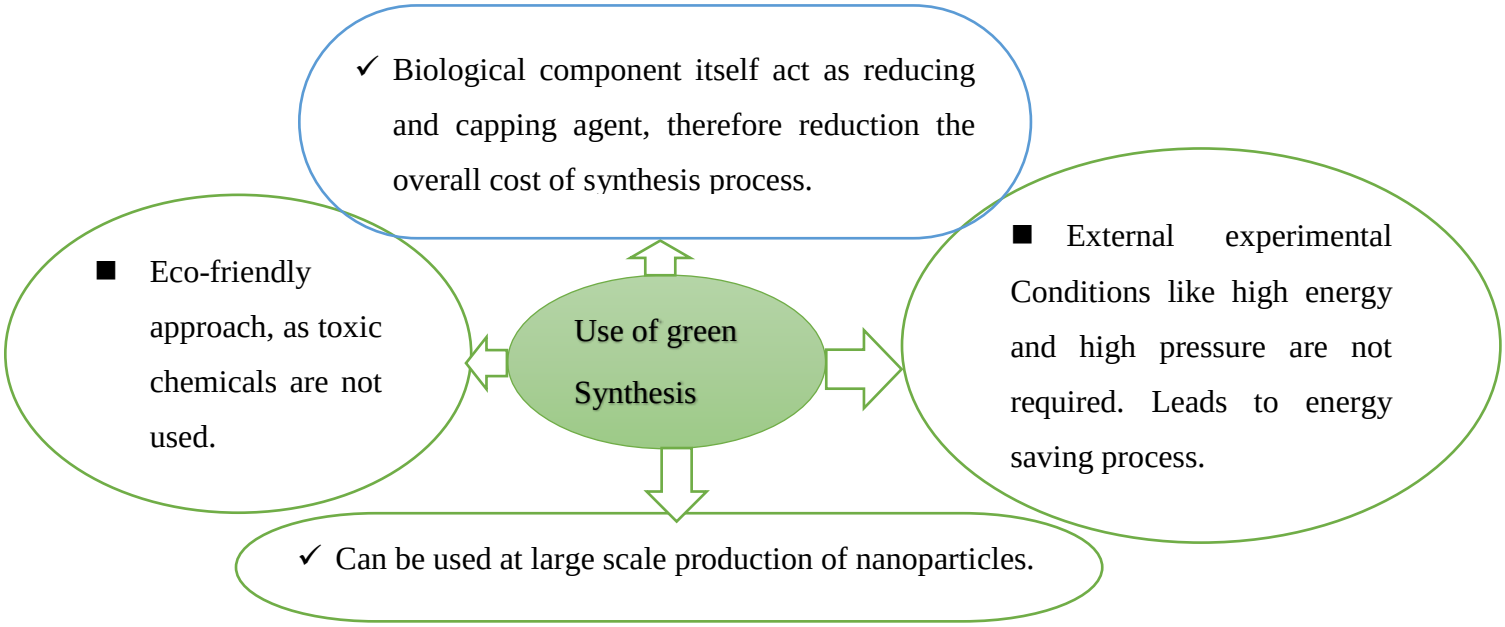

Figure 3: Key merits of green synthesis methods [49].

2.4 Need for green synthesis

The biosynthesis of nanoparticles is a bottom-up approach in which the primary reaction is reduction/oxidation. As the cost of physical and chemical methods rose, so did the need for nanoparticle biogenesis. Frequently, the chemical production process results in the presence of some of the toxic substances absorbed on the surface, which may have a negative effect in medical applications [50]. This is not an issue for biosynthesized nanoparticles created by the green synthesis approach. So, in search of cheaper nanoparticle production methods, scientists used microbial enzymes and plant extracts (phytochemicals), which have antioxidant or reducing properties and are often responsible for the reduction of metal compounds into their respective nanoparticles. Green synthesis outperforms chemical and physical processes because it is cost-effective, ecologically benign, easily saleable for large-scale synthesis, and does not require high pressure, energy, temperature, or toxic chemicals [51].

2.4.1 Synthesis of iron oxide nano particles from plant extracts

One of the first initiatives was utilizing plants to synthesize nanoparticles. The manufacture of nanoparticles using various plants and their extracts may be superior to other biological synthesis processes, which necessitate exceedingly complex procedures for maintaining microbial cultures. However, synthesis of nanoparticles using plant extracts is the most adopted method of green, ecofriendly manufacturing of nanoparticles and has the special advantage that the plants are widely distributed, inexpensively available, and much safer to handle in Ethiopia [52]. Plant extracts also contain bioactive polyphenols, alkaloids, proteins, sugars, phenolic acids, terpenoids, and other chemicals that play a crucial role in reducing and subsequently stabilizing metallic ions [53].

2.4.2 Mechanism of iron oxide nanoparticles synthesis

Plant extracts contain secondary metabolites, and phytochemicals operate as both reducing and stabilizing agents in metal nanoparticle synthesis, making them ideal bio resources for synthesizing iron oxide nanoparticles. The most important phytochemicals in plants are phenols and flavonoids, which can be found in a wide range of plant components such as shoots, leaves, stems, flowers, roots, and fruits. The phenolic compounds contain both hydroxyl and ketone

groups. Nanoparticles synthesized utilizing this green technology increased in stability, reduced agglomeration and deformation of the nanoparticles, and allowed for the adsorption of phytochemicals on the surface of the nanoparticles, which raised the reaction rate of nanoparticles [54, 55].

Depending on the iron precursor used to generate the iron oxide metal, electron-rich biomolecules containing hydroxyl groups (-OH) can effectively reduce iron ions from the trivalent oxidation state Fe^{3+}. The characteristics of the produced nanoparticles are mostly determined by discrete parameters such as plant extract type, volume ratio of the extract, and metal salt solutions. [6, 56].

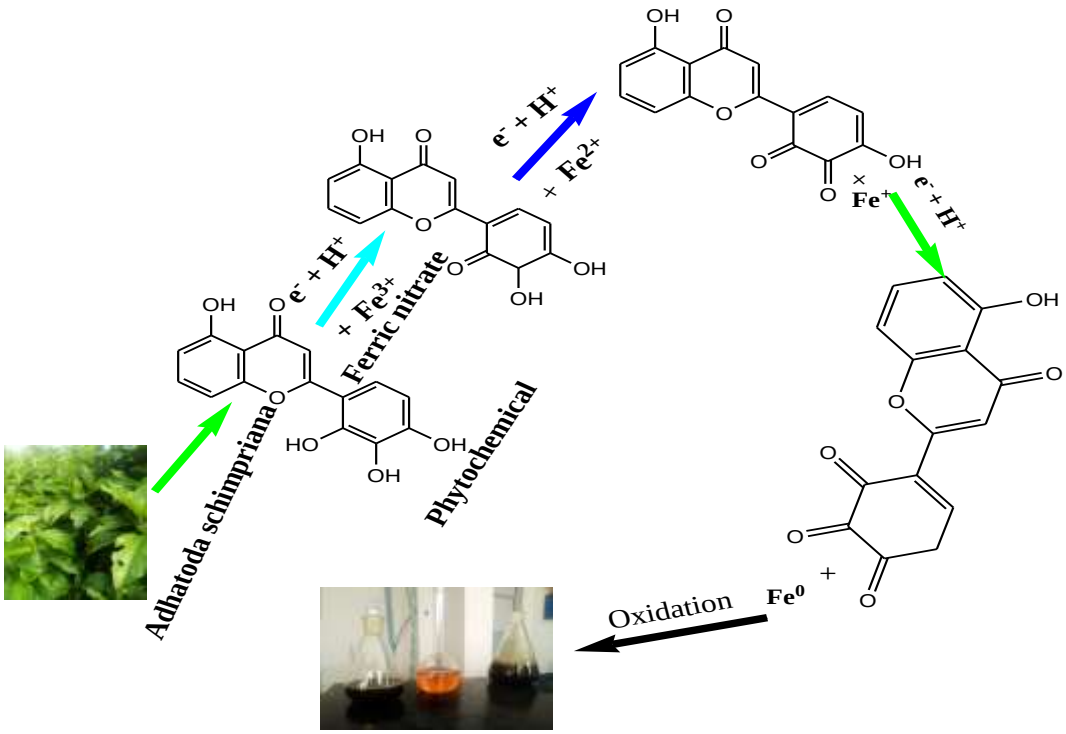

Figure 4: Mechanism of iron oxide nanoparticles synthesis [57]

2.5 Applications of iron oxide nanoparticles

Fe_2O_3 nanoparticles are efficient photo catalysts that absorb visible light. TiO_2, a common photo catalyst due to its high 3.2 eV band gap, absorbs UV light at 380 nm. While Fe_2O_3, an interesting n-type semiconducting material with a band-gap of 2.2 eV, is a viable candidate for photo

degradation in visible light conditions, Fe_2O_3 nanoparticles surpass TiO_2. Fe_2O_3 nanoparticles perform better. Photo catalytic performance over TiO_2 can be attributed to the significant production of electron-hole pairs created by narrow band-gap irradiation [58, 59]. Several Fe (III) oxide species, particularly Fe_2O_3 and FeOOH, have been proposed to breakdown organic pollutants and lower their toxicity due to their increased photo catalytic action [60]. Fe_2O_3 nanoparticles are one of the prospective materials for photo catalytic applications because of their low band gap energy [61], Chemical stability, high surface area, light absorption up to 600 nm, and efficient electron excitation of Fe_2O_3 nanoparticles from the valence band to the conduction band [62]. Because of their lower band gap (2.2 eV), Fe_2O_3 nanoparticles can participate in Fenton reactions as Fe ion precursors as well as photo catalysts under visible light As a result, Fe_2O_3 nanoparticles can be employed to degrade dyes while also having antimicrobial properties [63].

2.6 Dyes and the sources of dyes

Dyes are colorful chemicals that are commonly used in the textile, printing, rubber, cosmetics, plastics, and leather industries to color their products, resulting in a large amount of colored wastewater. The textile industry uses the most dyes for fiber dyeing. Dyes are chemical compounds that bind to textiles or surface shells to impart color. Depolarization of wastewater from textile and industrial sources. Industries is a severe concern for ecological managers since dyes are water-soluble and generate very bright colors in water with acidic properties [59, 64].

Dyes come from a variety of sources, including textiles, printing, paper, carpet, plastics, and leather. These dyes are consistently detected in industrial waste and eventually end up in bodies of water. Dyes are discharged into wastewater from a variety of industrial sources. Textile manufacturing and dyeing companies utilize a wide range of colors and dump these dye pollutants into the environment as wastewater effluents. These colors are highly toxic and even carcinogenic to microbial populations and mammalian species; thus, they must be cleaned from wastewater before it is discharged into bodies of water. Dyes are stable to light and not biologically degradable due to the presence of functional groups comprising nitrogen, aromatic rings, and conjugated double bonds; they are resistant to aerobic digestion and represent one of the most difficult groups to remove from industrial effluent. Dyes are stable to light and not

biologically degradable due to the presence of functional groups comprising nitrogen, aromatic rings, and conjugated double bonds; they are resistant to aerobic digestion and represent one of the most difficult groups to remove from industrial effluent [65].

Figure 5: The pollutant and affected water body by organic dyes [66].

2.6.1 Methylene blue dye

Methylene blue is a cationic dye with the chemical formula $C_{16}H_{18}N_3SCl$ with a molecular weight of 319.85 g/mol [67, 68].

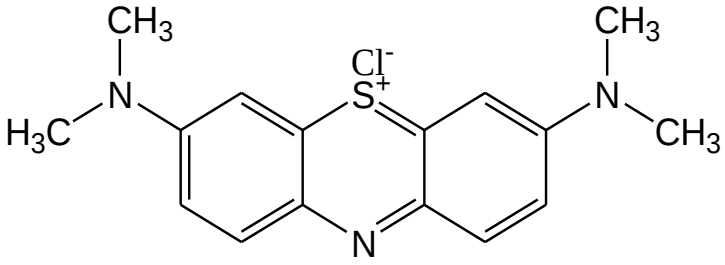

Figure 6: Chemical structure of methylene blue dye [67].

At room temperature, methylene blue dye is a solid, odorless dark green powder that turns blue when dissolved in water. It's an aromatic, heterocyclic compound. One or more carbon atoms in the backbone of the molecule are replaced by nitrogen, oxygen, or sulfur atoms [69]. Methylene blue ingestion generates a burning sensation in the mouth and may result in nausea, vomiting,

diarrhea, and gastritis. Once inhaled, it can cause rapid, difficult breathing. An accidental overdose produces chest and stomach pain, severe headaches, profuse sweating, methemoglobinemia, and painful urination. Currently, considerable volumes of MB dye from various sectors are dumped into bodies of water without treatment. As a result, researchers have expressed an interest in removing MB dye from polluted water bodies. A low-cost, environmentally friendly, and efficient water treatment technology, such as photo catalytic degradation of methylene blue dyes, considers tacking the problem [69, 70].

2.6.2 Dye removal techniques

Dyes are frequently used in the textile, plastic, leather, cosmetic, paper, culinary, and pharmaceutical industries to color the completed product [66, 71]. There are various common methods for eliminating color from industrial wastewater (effluents). These include biological treatment, electro dialysis, zonation, coagulation/flocculation, solid phase adsorption, membrane separation, electrochemical oxidation, ultrafiltration, sorption-floatation, and Fenton/Photo-Fenton oxidation. However, there are substantial downsides to these approaches, including: Biological treatments involve a long reaction time and emit unpleasant scents. Incineration can produce dangerous and volatile gases. Ozonation has a limited half-life, and its stability is strongly impacted by pH, salts, and temperature. Expensive, ineffective, and generate massive amounts of sludge and pollutants [72]. To efficiently remove dye from water systems, unique and specialized treatment technologies are usually required, such as photo catalysis and sophisticated oxidation procedures. [73] .

2.6.3 Mechanism of the Fe_2O_3 nanoparticles photo catalysis process.

Iron oxide, an n-type semiconductor with a direct and narrower band gap in the near-UV spectral region (2.2 eV), has significant electron mobility [74]**.** Iron oxide's electrical structure enables photo catalytic activity, giving it outstanding multifunctional properties. When iron oxide is exposed to UV light with an energy equal to or greater than the band gap (Eg), excited electrons go to the conduction band (e^-CB), leaving holes in the valence band (h^+ VB) (see Figure 7). In the presence of water and oxygen, two photochemical processes occur on the surface of iron oxide. The first involves photo-induced positive holes in oxidation, and the second involves

photo-induced negative electrons in reduction. In these reactions, highly reactive oxygen species (OH^- and O^{-2}) are created for the photo catalytic efficacy of iron oxide [75].

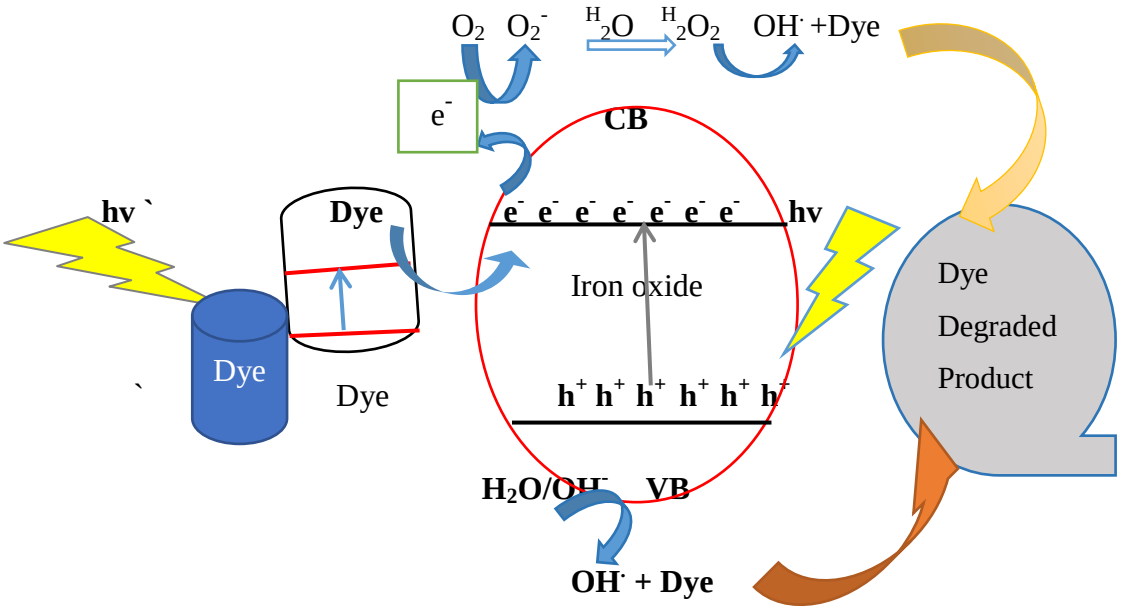

Figure 7: The proposed conduction and valence band diagram [76].

On the valence band

$FeO + hv \rightarrow h^+ + e^-$

$h^+ + H_2O \rightarrow OH\cdot + h^+$

$h^+ + OH^- \rightarrow OH\cdot$

On the condaction band

$e^- + O_2 \rightarrow O^{2-}$

$2O_2^- + h^+ \rightarrow HO_2\cdot + O^{2-}$

$HO_2\cdot + HO_2\cdot \rightarrow H_2O_2 + O2$

$H_2O_2 + e^- \rightarrow HO^- + OH\cdot$

$H_2O_2 + O^{2-} \rightarrow OH\cdot + OH^- + O_2$

$H_2O_2 + h^+ \rightarrow 2OH\cdot$

Organic dye + $OH\cdot \rightarrow CO_2, H_2O$ and inorganic ions.

Photo-excited electrons produce superoxide anion radicals (O^{2-}), which can generate additional H_2O_2 and OH radicals. The oxygen vacancies operate as traps for photo induced electrons, momentarily inhibiting the recombination of photo generated electron-hole pairs. The photo

generated electrons then attack the dissolved oxygen, forming surface-bound superoxide anion and hydroxyl ions, which are also responsible for dye mineralization in the photo catalytic reaction. The produced OH radical breaks several bonds in the dye (C-N, C=N, C-S, N=N, C-C, etc.) and converts it into CO_2, H_2O, and inorganic ions ($NH4^+$, NO^{3-}, SO_4^{2-}, Cl^-) [77]. The extremely reactive oxygen species ($OH^\cdot$ and O^{2-}) are produced on the surface of nanoparticles, specifically iron oxide. Since employing this extremely reactive $OH^\cdot$ (radical) to convert methylene blue dye into CO_2, H_2O, and inorganic ions [78].

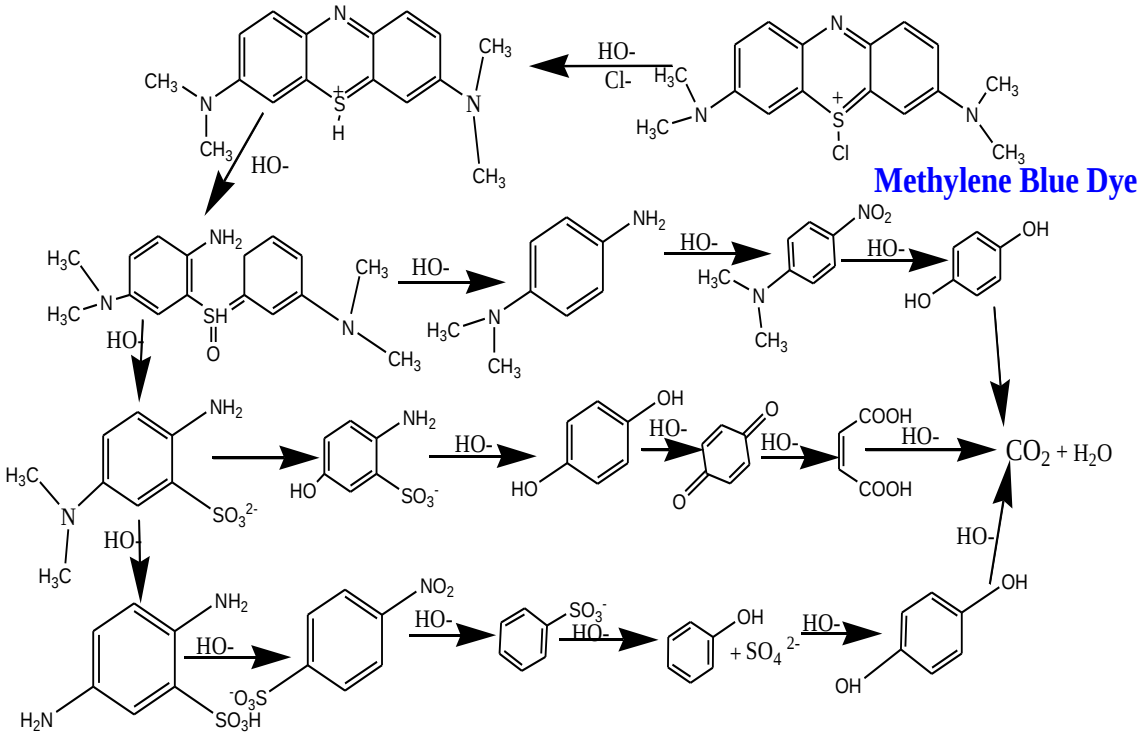

Figure 8: The reaction mechanism of the mineralization of methylene blue (MB) dye [79].

2.7 About *Adhatoda schimperiana*

Medicinal plants have been used for centuries in almost every civilization on the planet. The World Health Organization has proved that herbal medicines serve the health needs of around 80% of the world's population, notably millions of people in the vast rural areas of developing countries [80] . In Africa, the usage of traditional medicine has endured over the years, and the last few decades have witnessed an increase in interest in traditional medicine and various alternative types of treatment in both developing and industrialized countries [81].

The Acanthacae (or Acanthus) family consists of 250 genera and 2500 species. This genus contains around 600 species dispersed in tropical and temperate climes; the majority are tropical plants or twining vines; some are epiphytes [82]. *Adhatoda schimperiana* is a plant in the Acanthaceae family. *Adhatoda schimperiana* is a common erect shrub that sprouts several branches from its base. It is relatively quick-growing and prefers altitudes of 8,000 feet or above [83]. It is a common shrub found in moist mountain forest, primarily near streams and rivers, in evergreen scrub on hill slopes, forest clearings, various plantations, waste land, or cultivated [84]. It is an erect shrub up to 4 m tall, stem woody and with internodes, leaves decussate, estipulate, simple, ovate-oblong in shape, inflorescence thyroid, with densely flowered spikes, corolla bilabiate white to creamy white, fruit [85].

Figure 9: *Adhatoda schimperiana* in its natural habitat [84].

2.7.1 Pharmacological medicinal use of *Adhatoda schimperiana*

The traditional use of *Adhatoda schimperiana* varies by geography and culture. For generations, the Hadiya people of southern Ethiopia have used it to control malaria, wounds, gonorrhea, rabies, and headaches [86]. In Bahirdar Zuria, Ethiopia, traditional healers employ *Adhatoda schimperiana* leaf paste locally to treat burns and arthritis, and the leaf juice orally to treat jaundice [84]. In some areas of Ethiopia, the dried root of *Adhatoda schimperiana* is traditionally used to cure seizures [87]. In North Wollo and Gonder, Ethiopia, *Adhatoda schimperiana* leaves have also been used to treat malaria, rabies, diabetes, wounds, gonorrhea, headaches, intestinal parasites, and coccidiosis [88]. In addition to the aforementioned items, *Adhatoda schimperiana* is traditionally used to treat bilirubinemia and intestinal parasites [89]

3 Material and methods

3.1 Description of study area

The study was conducted in the North Wollo Zone, namely at Woldia town. Woldia, the largest town in North Wollo zone, is approximately 520 kilometers north of Addis Abeba in the Amhara region. Woldia town has an elevation of 2112 m above sea level and the average annual minimum and maximum temperatures, rain fall and relative humidity are 7 ^{o}C to 27 ^{o}C, 1.2 mm and 414.8 mm and from 40 to 74% respectively.

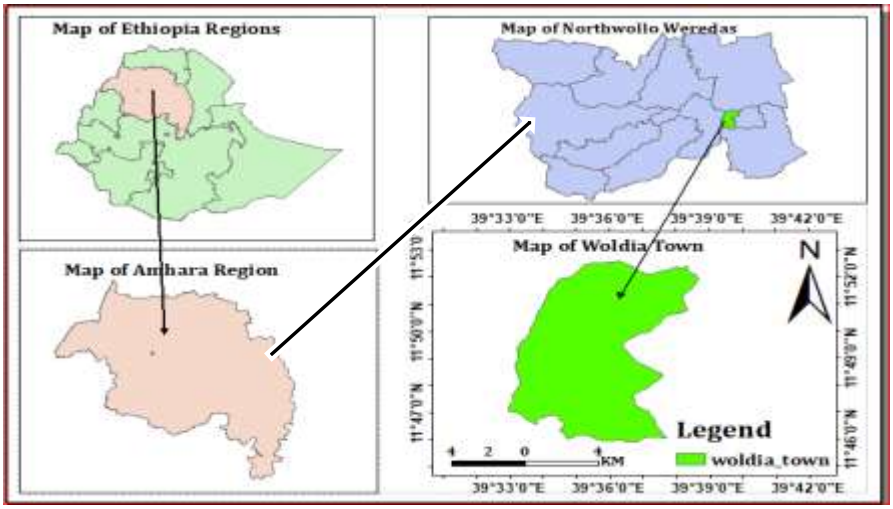

Figure 10: Map of the study area

3.2 Materials

3.2.1 Reagents and Chemicals

Ferric nitrate (Fe $(NO_3)_3 \cdot 9H_2O$, 98%, India), Ferric chloride ($FeCl_3$ 98%, Maharashtra. India), Hydrochloric acid (HCl, 35%, India), Sodium hydroxide (NaOH, 99.8%, China), Iodine (I_2, 99.8%), Methyl Blue dye (India), Potassium Iodide (KI, 99.71%, India), Distilled water, Ethanol (96%, Addis Ababa, Ethiopia) and Gentamycin were used in this study.

3.2.2 Apparatus and Instruments

The apparatus and the instruments used for this study were: Polyethylene plastic bag, What man No 1 filter paper, droppers, aluminum foil, test tubes, test tube rack, watch glasses, Crucible, Measuring cylinders, Pipette, hotplate, volumetric flasks, Erlenmeyer flask, grinder, beakers,

Spatula, disk, washing bottles, reagent bottles ,cuvette, centrifuge tubes, Analytical balance (FA2104), pH-meter (AD8000 PH/MV/EC/TDS and temperature meter), Centrifuge (12HOLE,India), magnetic stirrer (MS7-H5O-S),Autoclave (AX-B122) refrigerator (LLR-450), Oven, Muffle furnace (FCD-3000), Biosafety cabinet (BSC-1300IIA2-X), incubator (DH4000LL),UV-visible spectroscopy (UV9000UV/VIS SPECTROPHOMETER), Fourier transform infrared (Jasco-FT/IR-6600A), X-ray diffraction (XRD-7000X-RAY DIFFRACTOMETER), thermo gravimetric (HCT-1) analysis, and BET (ANOVA 4000e Instruments) analysis.

3.3 Methods

3.3.1 Collection and preparation of *Adhatoda schimperiana* plant

Adhatoda schimperiana leaves were collected from their native habitat in December 2016 E.C., Woldia town, near mugad, using a random sample approach in a polyethylene plastic bag. It was taken from three locations around "St. Micaal Church, Maksegno Gebeia, and Mugad" to limit the sample's geographical component. The sample was delivered to the chemical laboratory with a clean plastic bag in the morning. Fresh *Adhatoda schimperiana* leaves were washed with tap water to remove dirt before being rinsed with distilled water. Then it was allowed to dry in the shade at room temperature for two weeks. The dried leaf was pulverized with a grinder to create a coarse powder that was utilized for extraction.

3.3.2 Aqueous extraction of *Adhatoda schimperiana* leaf

An aqueous extract of the leaf was prepared by combining 2 g of *A. Schimperiana* dried leaf powder with 100 mL of distilled water in an Erlenmeyer flask and placing it on a magnetic hotplate with a stirrer (1200 rpm) at 80 °C for 30 minutes. Following cooling, the solution was filtered through what man No 1 filter paper and centrifuged for 40 minutes at 4000 rpm. The resultant fine solution was kept at 4°C for future use [90].

3.4 Qualitative analysis of phytochemicals

The presence of several phytoconstituents in aqueous extracts of *Adhatoda schimperiana* leaf was examined through phytochemical analysis utilizing standard chemical methods [91, 92].In this work the extract was tested for flavonoids, alkaloids, tannins, saponins, and phenols.

3.4.1 Test of alkaloids

Wagner's Test: Place 4 mL of plant extract solution in a test tube, and then add 5 drops of Wagner's reagent (1 g iodine and 3 g potassium iodide dissolved in 50 mL distilled water). After vigorous shaking, a reddish-brown precipitate was produced [93].

3.4.2 Test for flavonoids

Alkaline Reagent Test: In a test tube, combine 4 mL of plant extract solution with 6 drops of 1 M sodium hydroxide solution. They noticed the vivid yellow color [94].

3.4.3 Test for tannins

In a test tube, 3 mL of plant extract was combined with 2 mL of distilled water and three drops of 10% $FeCl_3$. During intense shaking, a blue-black color was detected [94, 95].

3.4.4 Test for saponins

Froth (foam) Test: 2 mL of plant extract was added into a test tube with 4 mL of distilled water, stirs rapidly for 20 seconds, and let stand for 10 minutes. The top layer of the mixed solution was then covered with sturdy foam about 1 cm tall [95].

3.4.5 Test for phenols

Ferric Chloride Test: Two drops of 10% ferric chloride ($FeCl_3$) were added to the plant extract solution (4 mL) in a test tube, shaken, and the dark green solution was observed [96].

3.5 Green synthesis of iron oxide nanoparticles

For the synthesis of iron oxide nanoparticles, the method of [97] was employed. To summarize, the optimum Fe $(NO_3)_3 \cdot 9H_2O$ solution (0.1 M) was mixed with optimum volume of plant extract solution (1:2) mL in a conical flask. The mixture was placed on a hotplate (optimum temperature was 60 °C) with a magnetic stirrer (200 rpm) at optimum pH 10 and observed for a dark color shift to dark brown after 60 minutes. The reaction mixture obtained after cooling was centrifuged for 40 minutes at 4000 rpm, and the pellet was washed three times with distilled water and ethanol to eliminate impurities. Finally, pure-wash pellet were collected in a crucible and dried at room temperature. Then, thermal stability tests were performed and the synthesized pellet was calcined in a muffle furnace at 660 ^{o}C for 2 hours to improve purity. This yielded pure pellets, which were maintained in sealed bottles under dry circumstances to employ alternative characterization.

3.6 Characterization of iron oxide nanoparticles (IONPs)

3.6.1 UV-VIS spectroscopy analysis of IONPs

To ensure the synthesis of nano iron oxide and plant extract was examined for optical absorption properties using a UV-Vis spectrophotometer with a wave length range of 200-800 nm with quartz cuvette and distillation water as the blank solution [98].

3.6.2 Thermo gravimetric analysis of IONPs

The thermal behavior was analyzed by thermo gravimetric (TGA) and differential thermal analysis (DTA) in the air using the TGA with the range from ambient temperature to 800 °C by taking 10 g [99].

3.6.3 FT-IR analysis of IONPs

The major chemical groups in the leaf extract, uncalicinated iron oxide nanoparticles, and calcined iron oxide nanoparticles were studied using an FT-IR spectrometer. The transmittance was measured between 400 and 4,000 cm^{-1} with the KBr pellet technique [100].

3.6.4 XRD analysis of IONPs

The uncalicinated and calcinated iron oxide nanoparticles' phase variety and grain size were determined using X-ray diffraction spectroscopy. The X-ray diffraction (XRD) pattern of iron oxide nanoparticles was obtained using a powder X-ray diffractometre with Cu Kά radiations (k = 1.54060 nm) in the 2θ range of 10 to 80 ^{o}C [101].

3.6.5 BET analysis of IONPs

The Brunauer-Emmett-Teller (BET) method was used to calculate the BET surface area and mean pore diameter of iron oxide nanoparticle samples based on the nitrogen adsorption-desorption isotherm. Before measuring nitrogen gas adsorption, the samples were vacuum degassed for at for 2 hours to eliminate any adsorbed species in the pores. Adsorption-desorption of the samples were then done by N_2 adsorption at 77 K [102] .

3.7 Photo catalytic activity

3.7.1 Photo catalytic degradation of methylene blue dye

Methylene blue dye was chosen as the model water pollutant for Photo catalytic degradation test by optimizing the following variable parameters: adsorbent dosage (20 -120 mg) with pH8,10 mg/l,0.1 M and 20 minute)) ,starting dye concentration (5-30 mg/L) with 0.1M,pH8 ,40 mg and 20 minute)) , pH (2-12) with 0.1M,40 mg,10 mg/l and 20 minute)), contact time (20-120 min) with 0.1M, 10 mg/l, 40 mg,pH9 and temperature (25 °C)). All solutions had their initial pH adjusted with 0.1 M NaOH or 0.1 M HCl. Centrifugation (4000 rpm for 10 min) was used to achieve the deterioration of the catalyst-MB equilibrium, followed by filtration. At the conclusion of each experiment, a tiny amount of the solutions (supernatant) was removed at a specified time, and the absorbance was measured using a UV-VIS spectrophotometer with the range of wavelength 200-800 nm [103]. The present photo degradability capability MB dye was estimated using Equation 1.

$$\text{Degradation } (\%) = \frac{\text{A0}-\text{At}}{\text{A0}}\text{x}100\% = \frac{Co-Ct}{Co}100\% \quad \ldots\ldots\ldots\ldots\ldots\ldots\ldots\ldots\ldots\ldots\ldots\ldots\ldots\ldots 1$$

Where, A_0 -the initial absorbance of MB dye, A_t - absorbance of MB dye after photo degradation at a time‘t’.

3.7.2 Recycling test of the iron oxide nano catalyst

An iron oxide nanoparticle catalyst's reusability was tested utilizing the dye degradation method under natural sunlight [104]. The 40 mg optimal value of iron oxide was added to a 100 mL beaker containing 30 mL of the 10 mg/l optimum concentration of MB solution. The mixture was agitated at room temperature for 30 minutes to reach an adsorption-desorption equilibrium between the catalyst and the MB dye. Then 5 mL of the mixture was obtained, centrifuged for 10 minutes, and its absorbance was measured between 200 and 800 nm. After the breakdown of the MB dye, the photo catalyst was centrifuged and rinsed with distilled water repeatedly before being dried at room temperature for one week before being used again. Using the same approach, photo catalytic degradation evaluations were carried out for three cycles under sunlight, and the percentage degradation was estimated for each trial using an equation (1) [105].

3.8 Anti -bacterial activity of iron oxide nanoparticles

The synthesized IONPs were evaluated for antibacterial sensitivity against Gram-positive (*Staphylococcus aureus, Salmonella*) and Gram-negative bacterial pathogens (*Escherichia coli*). The agar well diffusion assay was used in this investigation. Colonies of several bacterial species were injected with selective media (Mannitol salt agar, Macckonkey agar) and incubated for 48 hours at 37 °C in an incubator [106]. In the biosafety cabinet, bacteria were distributed evenly over the Muller-Hinton Agar substrate using a sterile spreader. The antibiotic disks (gentamycin as a positive control and distilled water as a negative control) with the produced calcined iron oxide nanoparticles in different concentrations (25 μg mL^{-1}, 50 μg mL^{-1}, 75μg mL^{-1}, 100 μg mL^{-1}(1:2)) and the concentration of crude leaf extract (25 μg mL^{-1} and 50 μg mL^{-1}) with 50 μL of volume each were placed at least 30 mm apart from the cultured petridish and incubated. Following incubation, the zone of inhibition around the disks was studied and measured with a ruler [107].

4 Results and Discussion

4.1 Phytochemical screening of the *Adhatoda schimperiana* leaf extract

The reddish-brown aqueous extract was derived from *Adhatoda schimperiana* leaf. The phytochemical contents of the leaf extracts were then examined, with the results shown in Table 1 and Figure 11 [108].

Table 1: Phytochemical screening of *A.Schimperiana* leaf extract.

No.	Secondary metabolites	Tests	Observations	Results
1	Phenols	Ferric chloride test	Dark green solution	++
2	Alkaloids	Wagner's test	Reddish brown precipitate	+
3	Saponins	Frothing (foam) test	A stable froth that persists for at least 2 min	++
4	Flavonoids	Alkaline reagent test	The observed intense yellow color.	+
5	Tannins	Ferric chloride	Blue-black coloration	++

+ = The sign indicates the presence bioactive component in Adhatoda schimperiana leaf extract.

++ = The sign indicates the presence highly bioactive component in Adhatoda schimperiana leaf extract.

The phytochemical examination of the aqueous extract of the chosen plant confirmed the existence of the phytoconstituents as shown in table 1, the *Adhatoda schimperiana* leaf extract was high in phytochemical elements such as phenols, saponins, flavonoids, tannins, and alkaloids were developed the color during the test was given in Figure 11. Recently, it was discovered that these bioactive compounds contain the OH^-, C=O-C, C=C, and C=O functional groups and act as reducing, capping, and stabilizing agents in the synthesis of nanoparticles [109].

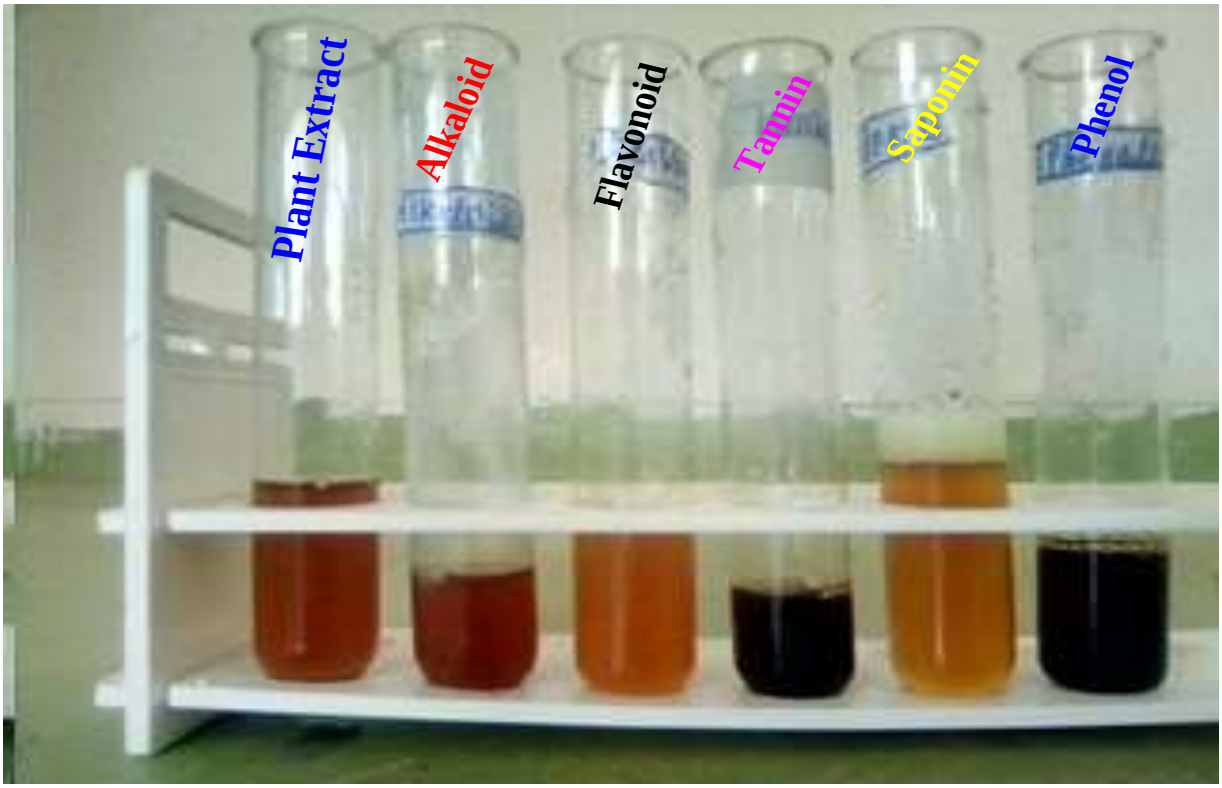

Figure 11: Phytochemical analysis of *Adhatoda schimperiana* leaf extract.

4.2 Optimization of important parameters for synthesis of IONPs

As previous investigations have revealed, examining physical factors including concentrations of precursor**,** volumes ratio of precursor and plant extract, effect of reaction time, effect of pH, effect of temperature and effect of plant extract during green synthesis of IONPs is critical for managing their stability. The absorption peak was kept between 200 and 800 nm wavelength for each parameter [110]. When a single parameter was optimized, the other values remained constant in each trial.

4.2.1 The effect of concentrations of precursor (Ferric nitrate)

The concentration of the precursor should be proportionate to the volume of plant extract used. In this study, 10 mL of different precursor concentrations (0.025, 0.05, 0.1, and 0.2 M) were mixed with 20 mL of leaf extracts to create each. 0.1 M was chosen because it produced a sharp peak that demonstrates the production of nanoparticles, as the intensity of the surface plasmon

peak has direct proportionality with the concentrations of synthesized nanoparticles in the solution [111]. The results obtained were in good agreement with current research, and an increase in intensity implies that more nanoparticles are synthesized [111].The results are depicted in Figure 27 (at appendix A) .

4.2.2 The effect of varying volumes ratio of precursor and plant extract

The types of biomolecules present in plant extracts, as well as the volume ratio, have a major impact on the production of IONPs. The volume ratio of ferric nitrate and plant extracts used in this study has a significant effect on the reduction of metal ions in their oxidation number (Fe^{3+} to Fe^{0}) [112]. To find the best volume ratio of ferric nitrate to plant extracts, numerous volume ratios of ferric nitrate to plant extract (1:1, 2:1, 1:2, 3:1, and 1:3) mL were reacted with varied volumes of precursors and extract. In this procedure, the 1:2 ratios in mL were the best number for achieving the smallest wavelength, the most intense peak, and a larger blue shift wavelength. This is due to phytochemicals included in the plant extract that are responsible for the bio reduction and stabilization of the IONPs [113] react with precursor. The result is shown in Figure 28 in (at appendix B).

4.2.3 The effect of varying reaction time

Reaction time is critical for the synthesis and stability of nanoparticles [114]. Thus, several reaction durations of 20 to 80 minutes were investigated, and 60 minute was shown to be an optimal time because the highest absorbance intensity of the UV-Vis peak was detected, indicating that all precursors were reacted with leaf extract and the reduction in metal ions was complete. The result is shown in Figure 29 (at appendix C).

4.2.4 The effect of pH

The pH was one of the parameters that affected the size, shape, and content of nanoparticles [114]. pH in an aqueous medium can have a significant impact on the progress of the metal ion reduction reaction, capping and stabilizing abilities, and consequently the growth of the nanoparticles [114]. For instance, the presence of OH^- ions in an alkaline pH environment may improve the reducing and stabilizing properties of the biomolecules in the leaf extract [115].

Thus, the pH range from 6 to 12 was treated to know the optimum pH value of IONPs for this study, and the result is given Figure 30 (at appendix D). Thus, at pH 10 a blue shift was observed that could be attributed to the decrease in the particle size. Therefore, pH 10 was considered as an optimum value for study. Above pH 10, it was not able to synthesize IONPs, as may be the high OH ion concentration hinders the process. The formation of IONPs occurs rapidly in the basic pH, it may be due to the ionization of the phenolic group present in the extract. The slow rate of formation and aggregation of IONPs at acidic pH could be related to the electrostatic repulsion of cations present in the solution [116].

4.2.5 The effect of temperature

In this study, the effect of temperature on the creation of IONPs was investigated, that the temperature had a significant impact on IONPs formation. The temperatures ranged from 25 ^{o}C to 120 ^{o}C were tested and an optimum value was found to be 60 ^{o}C. As shown in Figure 31 (at appendix E), there were sharp and intense SPR peaks of synthesized IONPs accompanied with a red shift along with temperature increase from 25 ^{o}C to 60 ^{o}C , whereas the broad and extremely weak absorption peak intensity of IONPs synthesized at 90 ^{o}C and 120 ^{o}C. As the temperature rises, the reactants are rapidly consumed, and smaller particles are produced [117].

4.2.6 The effect of plant extract

The influence of plant extract on the synthesis of IONPs was investigated, and it was discovered that the amount of plant extract had a significant impact on IONPs formation. The plant extract ranged from 2 to 6 g were implemented and the optimized amount was found to be 2 g. As shown in Figure 32 and Table 5 (at appendix F & G respectively), there were strong and powerful surface plasmon resonance (SPR) peaks of manufactured IONPs accompanied by a blue shift, and the amount of plant extract decreased from 6 to 2 g when the peak shift in blue said the nanoparticle size might be decreased that enhance the surface area of synthesized IOPNs [118].

4.3 Characterization of the synthesized samples

4.3.1 UV-Vis absorption spectral analysis

UV-Vis spectroscopy is one of the most commonly used easy and sensitive techniques for detecting nanoparticle formation [119]. The UV-Vis spectra of synthesized IONPs were measured at room temperature and ranged between 200 and 800 nm. The generated IONPs showed a distinct surface plasmon resonance (SPR) band in the 395–430 nm spectral range. The extract, ferric nitrate, and synthetic iron oxide all exhibited UV-Vis absorption bands at 426, 416, and 397 nm, respectively. As indicated in Figure 12. The shift from 416 nm to 397 nm (by 19 nm) was shown to create nanoparticles at the optimal wavelength. The results are in line with the previously reported IONP values [120].

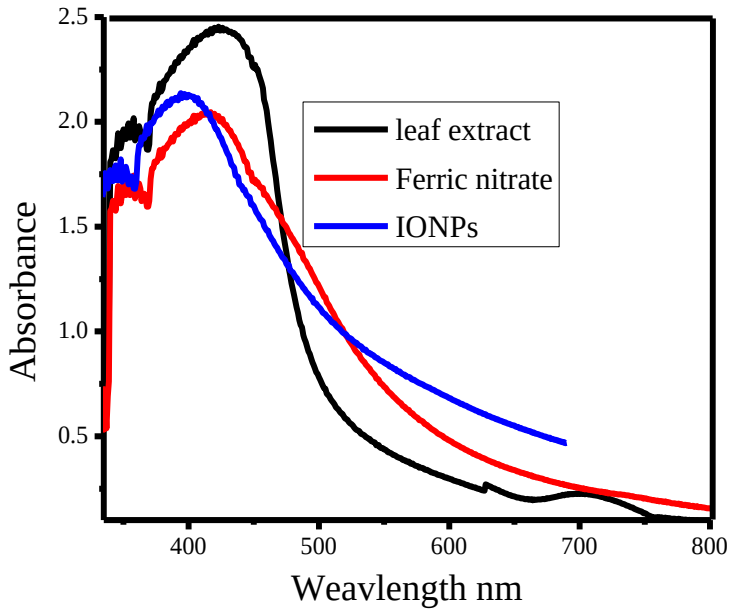

Figure 12: UV-Vis absorption spectra of extract, ferric nitrate and IONPs.

4.3.2 The band gap energy calculation of IONPs

The direct energy band gap of the synthesized IONPs was determined using the Tauc equation as given in equation 2:

$$\alpha h v = A(hv - Eg)^{1/2} \dots \dots \dots \dots 2$$

In this equation, α represents the absorption coefficient, h is Plank's constant, ν is the vibration frequency, A is constant, and Eg is the band gap.

Tauc plots were created by extrapolating UV-Vis data and plotting of hν (energy) on the X-axis and $(\alpha h\nu)^2$ on the Y-axis [121]. Based on the Tauc figure, the band gap energy of the adsorption edge wavelength of IONPs was measured and the result was found to be 2.18eV as shown in Figure 13. The shift of absorption edge of IONPs to a longer wavelength was resulted in smaller band gap energy. Thus smaller band gap of the IONPs might have a vital implication for various industrial applications as well as medical applications by photo catalytic activity and antibacterial activity [122].

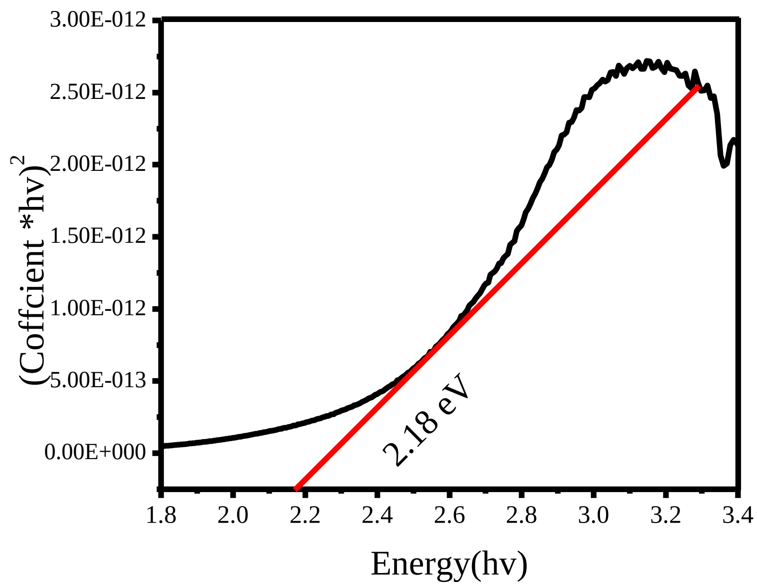

Figure 13: Tauc plot of IONPs for direct band gap calculation.

4.3.3 Thermo gravimetric analysis of IONPs

The results of thermo gravimetric analysis and differential thermal analysis (TGA/DTA) are in good accord with the findings related to the formation and decomposition phases that occur during heat treatment of synthesized IONPs. Thermal analyses were done between 800 °C and room temperature. The IONPs were heated in an air environment in an alumina crucible at a rate

of 10 °C/min to perform TGA. The thermal analyses (TGA/DTA) of synthetic iron oxide with Fe^{3+} = 0.1 M are shown in Figure 14. The operating temperature ranges have three different mass loss stages. The initial phase of weight loss, which accounted for approximately 1.0409% of the total weight loss, happened gradually between 44 and 227 °C. This weight loss is explained by the elimination of water that was present on the IONP surface. Our prepared sample contains combustible organic compounds, which is the reason for the mass loss of 2.025% at 228–593 ^{o}C in the second stage. The third stage represents a slight weight loss (0.346%) that takes place between 600 and 660 °C and is caused by the produced chemicals' transition phase. The curve becomes parallel to the temperature axis after 660 °C, high lighting the great stability of IONPs. There is no associated signal with the thermal processes of IONPs in the TGA curve confirming the crystallization and phase transition of IONPs associated with them. Moreover, no further modifications were observed after 660 °C, suggesting that the synthesized IONPs were extremely thermally stable (Figure 14) [123]. On the other hand, DTA enabled us to find endothermic peaks that; first, second, and third endothermic peaks were found around 105 ^{o}C, 283 ^{o}C and 600 to 660 ^{o}C, respectively.

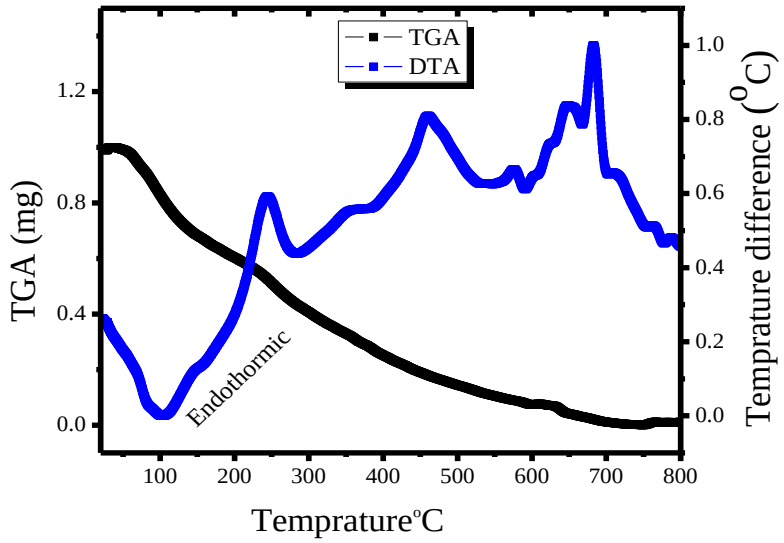

Figure 14: TGA and DTA analysis of synthesized IONPs.

4.3.4 FT-IR spectroscopic analysis of IONPs

The surface functional groups of produced IONPs were investigated using FT-IR over a spectral range of 4000-400 cm^{-1} at room temperature with the goal of identifying the functional groups (such as phenol, saponins, flavonoid, alkaloids, carbonyl and hydroxyl) responsible for reducing and stabilizing agents. The result of the present study is given in Figure 15 a. Hence, a broad absorption band, most likely in the range of 3600-3100 cm^{-1}, corresponds to the hydroxyl groups (O-H) stretching ,which it suggested the presence of alcoholic or phenolic groups in the leaf extract with a wide diversity of hydrogen bonding [124].The peak intensity of ~3378 cm^{-1}(Figure 15 b) indicates the coordination of O-H groups with IONPs (Figure 15 a). The strong and sharp peak at 1611 cm^{-1} indicates the presence of carbonyl (-C=O) groups, which are responsible for capping and stabilizing agents (Figure 15 a).The C=O stretching changed to 1610 cm^{-1} (Figure 15 b), 1622 cm^{-1} (Figure 15 c), and got shorter, indicating that the carbonyl groups were capped in the produced nanoparticles. The brief peaks at 1622 cm^{-1} and 1383 cm^{-1} revealed the presence of -C=C functional groups and N-O in the extracts, respectively. There was also a spectral band at 1380 cm^{-1}, which corresponds to the symmetric stretching of nitrate species in IONPs. The absorption peak at 1032 cm^{-1} could be attributed to C-N stretching in primary amine or to the C-O stretching vibration of phenolic groups (Figure 15 c). A brief peak occurred at 956.4 cm^{-1} (Figure 15 a), indicating the presence of polyphenols, carboxylic acid, polysaccharide, amino acid, and proteins in the leaf extract. The absorbance peak was then lowered to 574.1 cm^{-1} and 443.3 cm^{-1}, indicating that the produced IONPs were well coordinated with these metabolites (Figure 15 c). A strong peak at 574.1 cm^{-1} indicates the typical absorption of the IONPs bond (Figure 15 b). The FT-IR spectrum confirmed the existence of active chemicals in the extract, which may greatly contribute to nanoparticle stabilization, as previously described [125, 126].

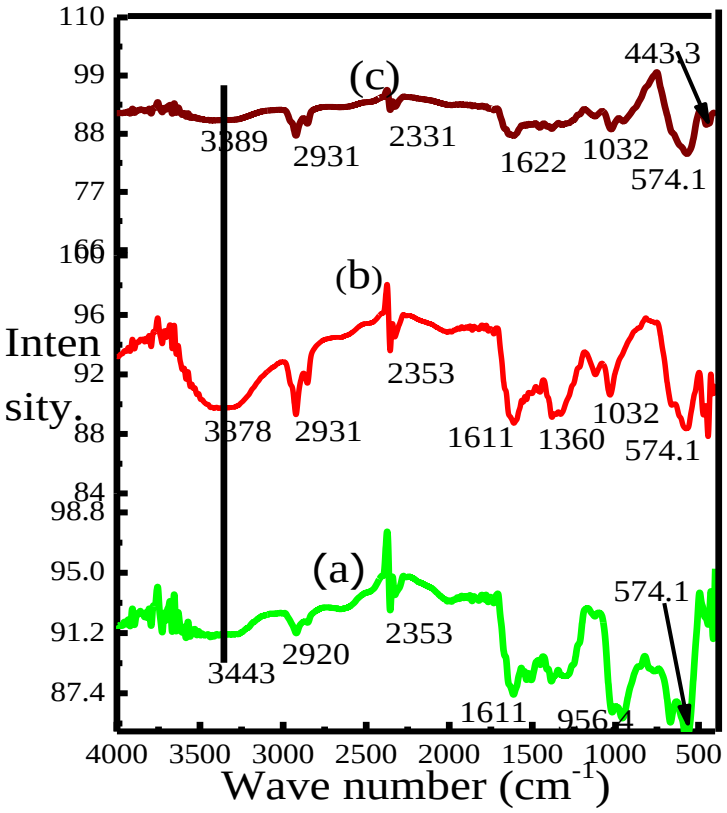

Figure 15: FT-IR spectra of the leaf extract (a), uncalcineate (b) and calcinated IONPs (c).

4.3.5 XRD analysis of IONPs

Using X-ray diffraction (XRD) at a scan rate of 3^{o}/min, the crystal structures and diffraction patterns of both calcinated and uncalicinated IONPs were identified. The patterns showed distinct peaks at 2θ, which corresponded to the crystal planes of the uncalicinated IONPs (Figure 16 a). The peaks ranged from 30.13^{o} to 34.19^{o}, 60.18^{o}, and 62.39^{o}. The joint committee on powder diffraction standards has suggested that these diffraction peaks are associated with the good crystalline structure of uncalicinated IONPs (JCPDS No: 025-1402) [127]. The additional many small peaks observed in the XRD pattern of uncalcineate IONPs may be contributed from the precursor ferric nitrate nine hydrate, water and phytochemicals, after calcinated of IONPs by 660^{o}c for 2h, there were a change in intensity peaks and slightly shift of diffraction angles observed. Specifically, the weak peaks looked at 24.1^{o}, 33.11^{o}, 43.31^{o}, 54.1^{o},57.31^{o} and 74.69^{o}

were related to the intense (012), (104), (0012), (2212) , (1115) and (3315) reflection (Figure 16 b). However, the intense peak at 35.77^{o} was observed well, it may be resulted from high in amount of the IONPs. It was in good agreement with the already reported value and with standard data card (JCPDS No: 033-0664) [125].The presence of metallic iron content on the iron oxide surface was indicated by the appearance of those peaks in the diffraction pattern. based on XRD analysis, the diffraction peaks of (206), (119), and (4012) were narrow and high-intensity when compared to uncalcineate iron oxide nanoparticles in Figure 16 a due to the effect of different impurities in uncalcineate FeO structures. Based on these findings, the majority of the impurities are found on the surfaces or the interface of the uncalcineate iron oxide structure. Some iron ion peaks were also not found in the XRD study due to limited dispersion and low metallic iron content. Using Debye-Scherer's equation [128], the average crystallite size was determined to be between 12.82 and 16.66 nm in size that is the average crystalline size to be 14.31 nm IONPs products. These results have good agreement with the previous study [129].

$$D = \frac{0.94\lambda}{\beta COS\theta} \ldots\ldots\ldots\ldots\ldots\ldots\ldots\ldots\ldots\ldots\ldots\ldots\ldots\ldots\ldots\ldots\ldots\ldots\ldots .3$$

Where, D = average crystallite size, λ is wavelength of X-ray beam (1.54056Å), θ is the Bragg diffraction angle in degree, β is full width at half maxima (FWHM) of XRD peak.

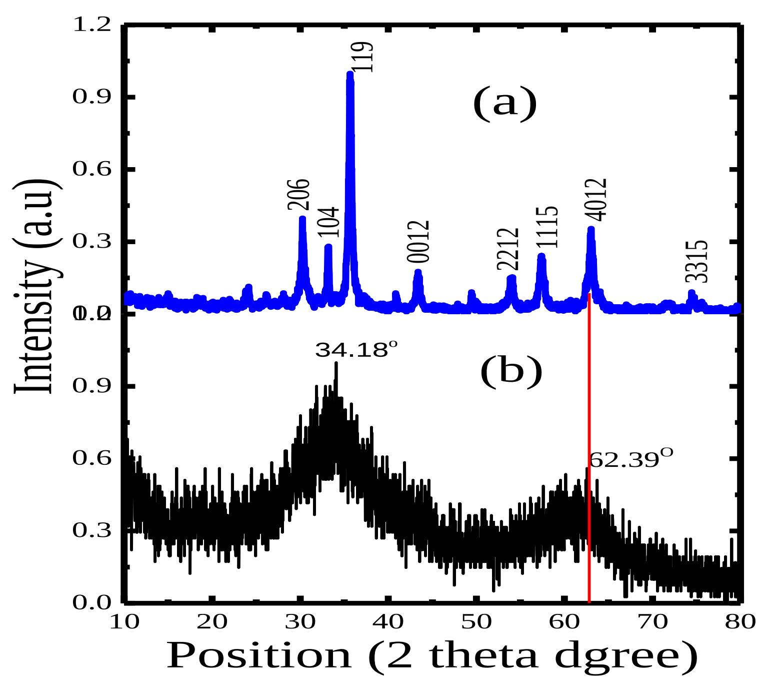

Figure 16: XRD pattern of calcinated (a) and uncalicinated (b) IONPs.

Table 2: The structural parameters of IONPs as obtained from XRD analysis.

2^{0} (degree)		
Hkl	Observed	JCPDS
012	24.1^{o}	24.2°
104	33.11^{o}	33.1°
119	35.67^{o}	35.7°
0012	43.31^{o}	40.9°
2212	54.1^{o}	54.1°
1115	57.31^{o}	57.6°
4012	63.04^{o}	62.5°
3315	74.69^{o}	75.5°

4.3.6 The BET analysis of IONPs

The uncalcineate IONPs' BET surface area and pore volume were determined to be 276.325 m^2/g and 5.46 cc/g respectively, with a pore diameter of 3.92 Å. Nonetheless, the calcined IONPs' BET surface area was determined to be 286.861 m^2/g, which is significantly more than the uncalcineate IONPs' maximum surface area, which has been reported by several researchers and is displayed in table 3.The resultant nanoparticle surface area is found in the of commercial Fe_2O_3 is 63 m^2/g [130]. Therefore, the obtained surface area is 4.55 times greater than the commercial one. Furthermore, measurements of the pore width and pore volume of calcinated IONPs were 1.81 Å and 4.57 cc/g, respectively, which supported the micro porous character of the pores. Therefore, the IONPs' increased specific surface area and micro pore structure could be advantageous for the material's possible catalytic use in a variety of applications. Furthermore, the calcinated IONP's predicted diameter of 14.31 nm supported the nano range.

Table 3: BET surface area of some of the published reports on IONPs.

No	Synthesis Method	BET surface area (m^2/g)	References
1	Green synthesis *camellia sinensis* leaf extract	22.5	[131]
3	Facile synthesis of porous α-Fe_2O_3 nano rods and their application in ethanol Sensors.	221.9	[132]
2	Synthesis of steel waste-based iron oxide nanoparticles.	325.02	[133]
	Green synthesized α-Fe_2O_3 nanoparticles using the leaf extract of *Spondias dulcis*.	190.84	[134]
3	Green synthesis *Peltophorum* leaf extract.	66.44	[135]
4	Chemical synthesis	79.2	[136]
5	Chemical synthesis	90.71	[137]
6	Green synthesis *Adhatoda shembriana* leaf extract of uncalcineate IONPs.	**276.325**	**This study**
7	Green synthesis *Adhatoda shembriana* leaf extract of Calcinate IONPs.	**286.861**	**This study**

4.4 Optimization of photo catalytic parameters

For each parameter, the decolorization and percentage dye degradation efficiency (removal efficiency) were calculated using equation (1) [129].

4.4.1 The effect of IONPs dose

The methyl blue (MB) dye degradation was assessed using the produced IONPs. In order to find out the optimum concentration, the effect of various amounts of synthesized IONPs (20, 40, 60, 80, 100, and 120 mg) was studied at constant pH (8), concentration of dye (10 mg/l), temperature (25 ^oC), and contact time (20 minutes). It was observed that increasing the catalyst dose from 20 to 40 mg enhanced the degradation rate. It indicates that the dose of iron oxide nanoparticles up

to 40 mg produces higher amounts of species having active sites (hydroxyl and superoxide radicals) on the synthesized IONPs surface and provides good photo catalytic degradation efficiency. However, the degradation performance decreases at further increases in the catalyst dose [63]. This could be due to an increase in turbidity of the working system that scatters solar radiation, delimits the photo excitation efficiency to activate the catalyst surface, and the photo catalytic activity decreases [63]. The obtained results showed that an optimum amount of catalyst for decolorization of the dye mixture was 40 mg, as greater than 89% of dye degradation was achieved [70].

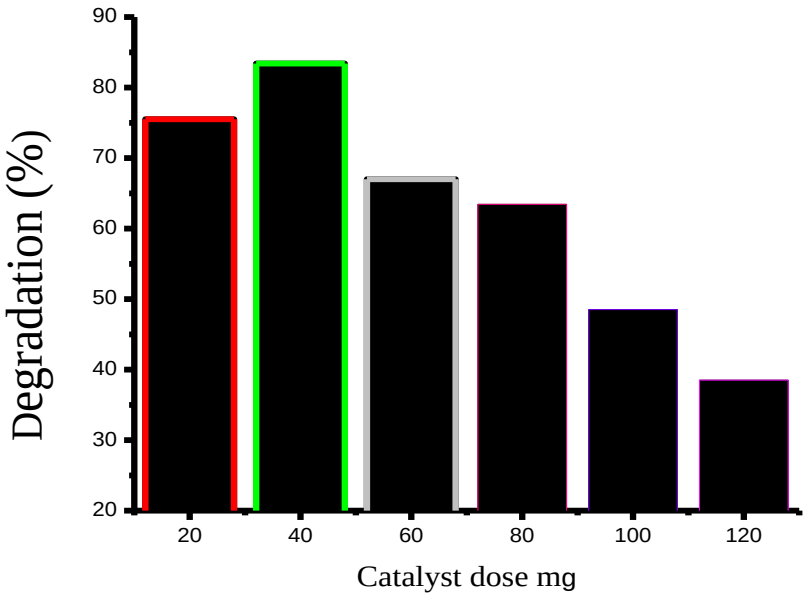

Figure 17: Effects of IONPs dose on MB photo degradation.

4.4.2 The effect of initial dye concentration

Other variables, such as PH (8), temperature (25 °C), catalyst dose (40 mg), and irradiation time (20 min), were held constant while different MB dye concentrations (10, 15, 20, 25, and 30 mg/l) were utilized independently to find the ideal amount of dye. As the dye concentration increased, the dye's efficiency of degradation reduced. This occurrence is caused by more dye molecules adhering to the catalyst's surface, which prevents photons from penetrating the iron oxide surface and reducing the number of active sites for the production of hydroxyl radicals [70]. More than

74.6% of MB dye (10 mg/l) was degraded, so that it was determined as initial optimal concentration (Figure 18).

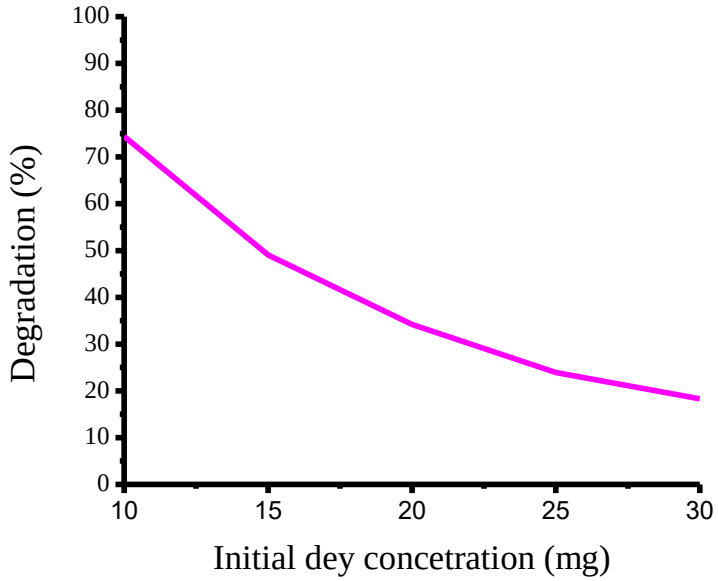

Figure 18: Effects of MB dye concentration on photo degradation.

4.4.3 The effect of pH and Point of zero charge

One of the main elements affecting the dye pollutants' ability to break down photodegradable is the pH of the working solution [138]. The determination of the point of zero charge (PZC) preceded the optimization process for the impacts of pH. The pH value at which the particle surface's net charge is zero or neutral is known as PZC. Six beakers, each with a different pH adjusted between 2, 4, 6, 8, 10, 12, and 0.1 M HCl and 0.1 M NaOH, each labeled pHi, were filled with 30 mL of 0.1 M NaCl. Following the addition of 40 mg of Fe_2O_3 nanoparticles and a 24-hour shake, the pH values of the supernatant in each vial were determined and assigned the letter pHf. The PZC was obtained from the intersection point of the plot of ΔpH (pHf – pHi) versus pHi (Figure 19). Below this value, the surface of the catalyst is positively charged and is always easier to adsorb an anion, whereas beyond this value, it is negatively charged particle surface so that it adsorbs a cation on a negatively charged surface[139].

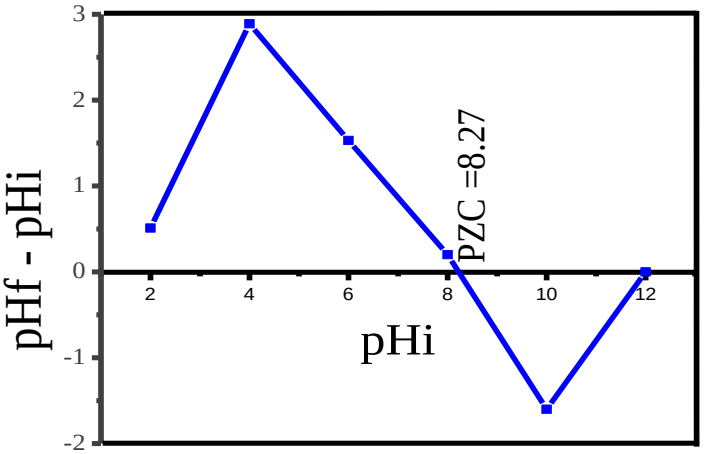

Figure 19: Determination of pH at point of zero charge.

The study employed 0.1 M HCl and 0.1 M NaOH solutions to regulate the pH of a 10 mg/l solution mixture of MB dye, which contained 40 mg of nano catalyst. The pH was calibrated to fall between 4, 6, 8.27, 9, 10, 11, and 12 before initiating the photo catalytic degradation process. The experiment on the effects of pH on dye degradation was then carried out using the photo catalytic technique, and the findings revealed that pH 9 had the maximum degradation efficiency of 95.71% [137]. Therefore, pH 9 was accepted as the optimized value of the working condition for photo catalytic degradation.

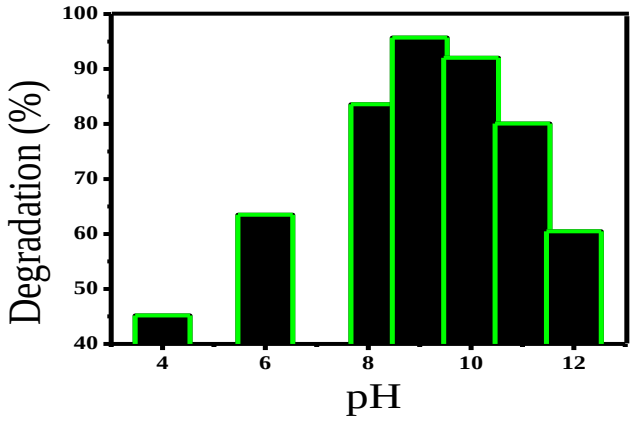

Figure 20: pH effects on percent degradation of MB dye.

As seen from Figure 20, at pH 4, the least effective photo catalytic degradation was observed. This low value results from a repulsion between the positively charged iron oxide nanocatalyst surface and the positive groups of the MB dye molecules, which reduces the photo degradation efficiency. Meanwhile, at pH values of 8.27 and higher, demethylation and photo degradation of methylene blue were noted in the presence of the Fe_2O_3 nanoparticle [63]. About 83.59% of the MB dye was partially decolorized and degraded at pH 8.27 at the start of the constant period. It has been established that when the pH is higher than 8.27 to 12, an excess of hydroxyl ions (OH^-) can cause the catalyst's surface to become negatively charged. These excess OH^-ions can then search for holes on the iron oxide surface and convert to hydroxyl radicals. As a result, the density of OH radicals and the coordination between the positive groups of MB dye were increased, which improved the photo degradation performance. However, the excess amount of OH caused the surface of the Fe_2O_3 nanoparticle to be hindered, causing the photo degradation performance to decrease from pH 11 to pH 12 [140]. The optimum pH value was obtained at pH 9 which the value was 95.71%.

4.4.4 The effect of irradiation time

Using 40 mg of iron oxide catalyst and 10 ppm of MB dye solution at pH 9 and room temperature, the effect of irradiation time on the degradation efficiency of the photo catalyst was investigated at time intervals ranging from 20 to 120 min for the catalyzed and from 20 to 200 min for the uncatalyzed MB dye, both under UV light. The result of the study has been given in Figure 21. The percent degradation was evaluated using equation 3 [141].

The percentage of dye degradation at 80, 100, and 120 minutes was 93.74%, 96.61%, and 97.13%, respectively. The dye mixture completely decolored after 120 minutes, and photo degradation was completed, allowing 120 minutes to be considered the ideal irradiation time. The current study's results are roughly comparable to those of the photo degradation of MB dye, which was completed at 120 minutes and resulted in 95% degradation by Fe_2O_3 nanoparticle [142].

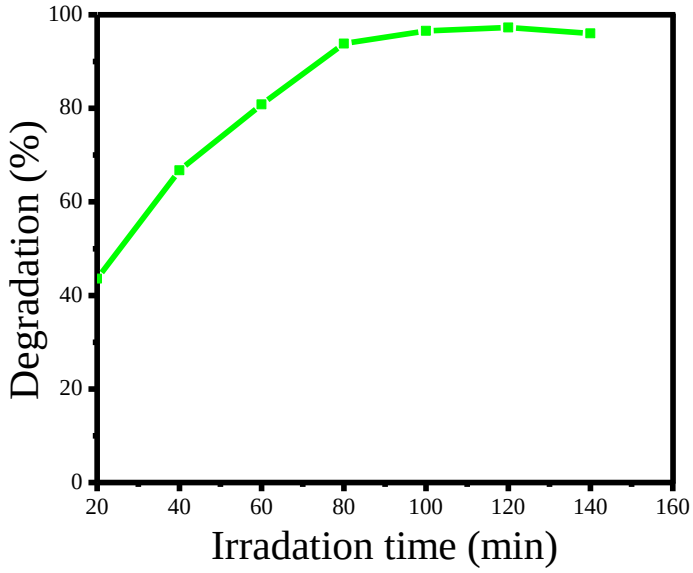

Figure 21: Effects of irradiation time on photo degradation of MB dye.

4.5 Photo catalytic degradation activity of calcinated IONPs

The degradation of MB was utilized to assess the iron oxide nanoparticle photo catalytic effectiveness under ideal conditions. After being exposed to an iron oxide catalyst for 20 to 120 minutes, the absorbance of MB dye at 664 nm was dramatically lowered, resulting in dye decolorization (Figure 22, 23 and table 6 at appendix H).

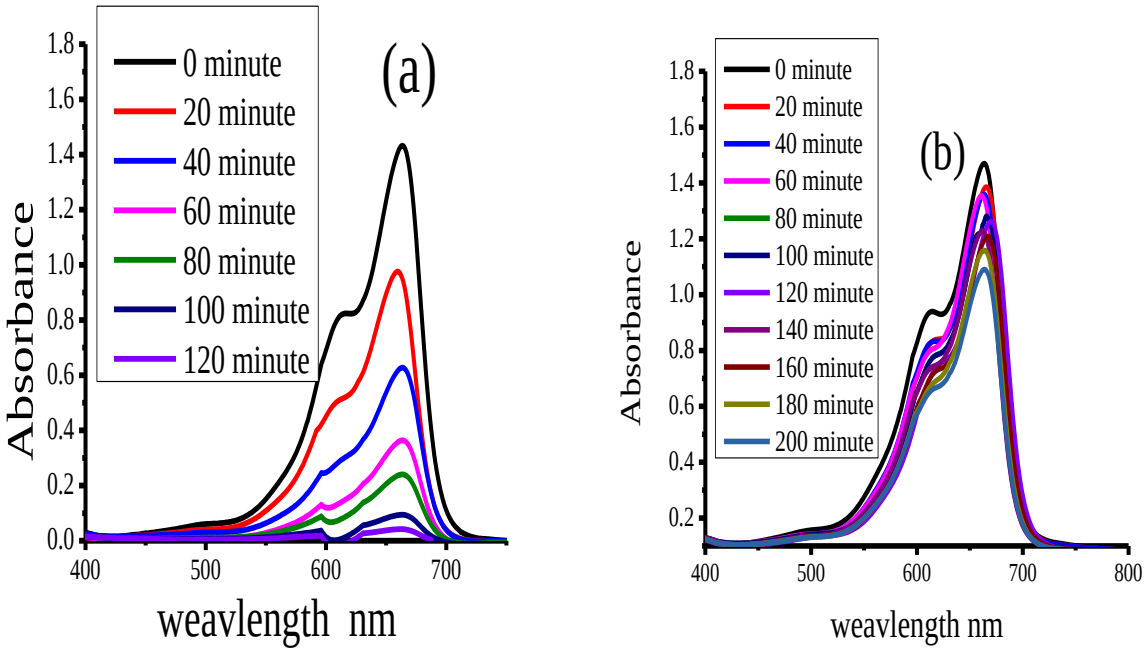

Figure 22: UV-Vis of MB dye catalyzed by Fe_2O_3 nanoparticles (a) and uncatalyzed MB dye (b).

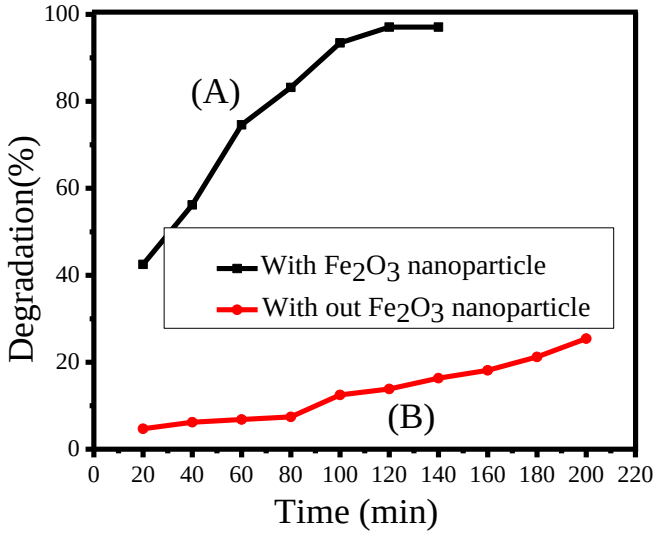

Figure 23: Photo catalytic percent degradation efficiency of MB dye.

The findings showed that an increase in illumination time boosted the iron oxide photo catalyst's effectiveness of degradation. After 120 minutes of irradiation, the dye combination catalyzed by Fe_2O_3 nanoparticles was completely decolorized, and more than 97.082% was photo catalytically degraded, while the dye catalyzed just by sunlight only saw approximately 25.431% degradation even after 200 minutes of irradiation. This data demonstrated the iron oxide catalyst's good efficacy in eliminating the MB dye pollution when it was generated using plant leaf extract [142]. The percent degradation of MB dye catalyzed and non-catalyzed by nanoparticles, respectively was illustrated (Figure 22 &23).

4.6 Re-usability of the IONPs

The reusability of the photo catalyst was progressively done, and the percent of degradation was determined after 120 minute of sunshine irradiation for three cycles [143]. The photo degradation results show 90.25%, 83.56%, and 70.34% of dye degradation in the first, second, and third cycles, respectively. It was illustrated by Figure 24.

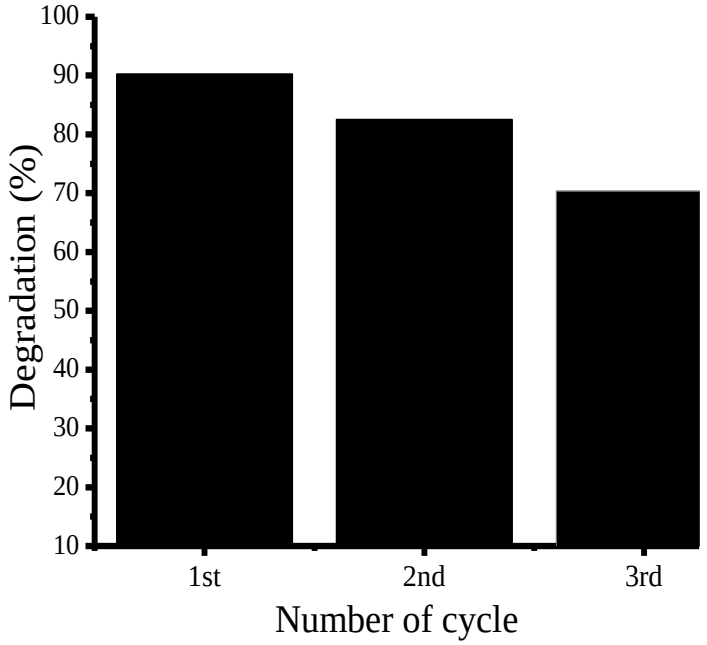

Figure 24: Cycling times of the photo degrading MB dye applying IONP catalyst.

Reusability of the catalyst is a key component of the photo catalytic process since it significantly lowers the expense of treating dye effluent. For photo catalytic runs, iron oxide nanoparticles were utilized to evaluate the stability of the photo catalyst. The results in Figure 24 indicated that the activity of iron oxide slightly decreased and MB degradation was achieved after three runs from 1st cycle (90.27%) to 3rd cycle (70.34%). Also, the photo catalytic activity of the samples only minimally decreases, due to the unavoidable loss of photo catalysts during the cycle processes [144].

4.7 Antibacterial activity

Using a well diffusion approach, the antibacterial potential of the produced IONPs containing *Adhatoda shembriana* leaf extract is evaluated against *Salmonella*, *Staphylococcus aureus*, and *Escherichia coli*. The results are displayed in table 6 and Figure 25.All examined bacterial strains were susceptible to the antibiotic effects differently to the green-produced IONPs. Because gram-positive and gram-negative bacteria have different structural compositions gram-positive bacteria have thicker peptidoglycan layers surrounding their cell walls, while gram-negative bacteria have thinner peptidoglycan cell walls the bacterial effect of IONPs was found to be greater for gram-negative bacteria than for gram-positive bacteria. IONPs synthesized from *Adhatoda schimperiana* aqueous leaf extract demonstrated the largest zone of inhibition against *Salmonella* (13.7 mm), *Escherichia coli* (18 mm) and *Staphylococcus aureus* (16 mm) at concentrations of 100 μg/l as well as the positive control (gentamycin) has zone of inhibition 21, 25 and 22 mm respectively since the zone of inhibition to each disk approach to positive control value. Similar findings on IONPs' antibacterial activity against *Salmonella* and *E. coli* have been previously documented in the literature [145].

The concentration of crude extract and IONPs synthesized using *Adhatoda schimperiana* aqueous leaf extract (mg/l).

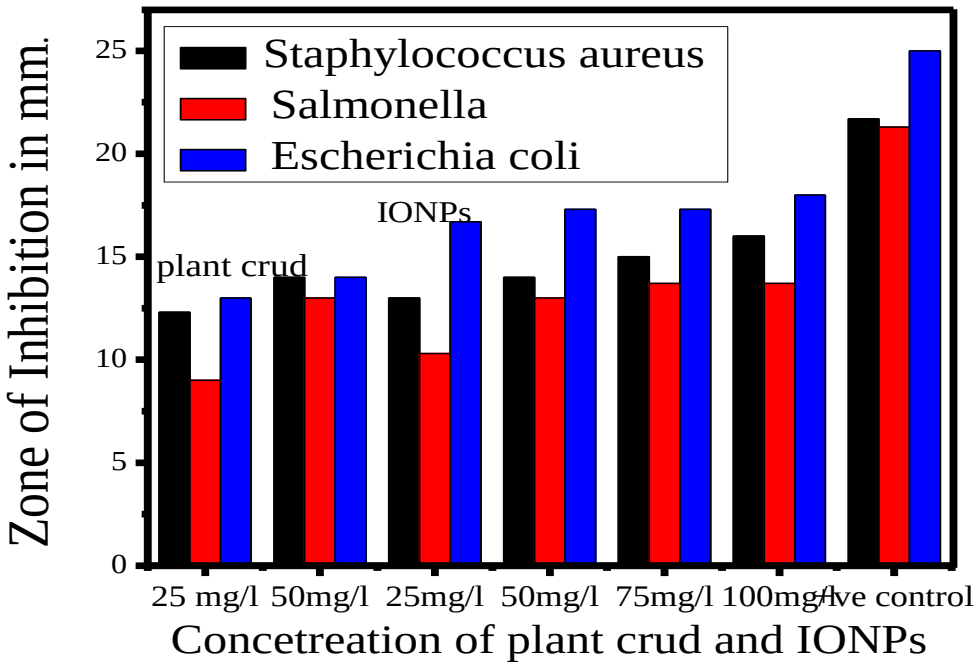

Figure25: Graphical representation of zone of inhibition of crude extract and IONPs synthesized using *Adhatoda schimperiana* aqueous leaf extract.

The mechanism of IONPs antibacterial activity may be explained by the way that smaller IONPs penetrate and break down membranes, causing cell lysis. Another theory regarding the potential mechanism of bacterial action of IONP is the release of H_2O_2 from their surface. The surface area of IONP has a significant impact on the production of H_2O_2, which enters cells and damages them, ultimately killing the bacteria. *Adhatoda shembriana* aqueous leaf extract had potential bio reducing and bactericidal activity against the studied bacteria since it contained alkaloids, flavonoids, tannins, saponins, phenolic groups, and amino acids. These compounds may find utility in biomedical applications [146].

Table 4: Zone of inhibition (mm) of crude extract and Fe_2O_3 nanoparticle synthesized using *Adhatoda schimperiana* aqueous leaf extract.

Bacterial pathogens		Zone of inhibition for crude extract of leaf		Zone of inhibition for IONPs					
Staphylococcus aureus	Trial	25 µg/l	50 µg/l	25µg/l	50µg/l	75 µg/l	100 µg/l	Gentamycin (+ve)	Water (-ve)
	1	12	14	15	17	16	19	22	-
	2	13	15	14	13	15	14.1	24	-
	3	12.2	13.1	10.5	12	14	15	19.5	-
	Mean	12.40±0.53	14.03±1.00	13.17 ±2.36	14.00±2.65	15.00±0.33	16.03±2.61	21.83±2.25	-
Salmonella	1	12	14	10	13	14	12	22	-
	2	5.5	12	10.2	14	14.2	15	20	-
	3	10	10	11	12	13	14	22	-
	Mean	9.17±3.33	12.00±2	10.40 ±0.51	13.00 ±1	13.73 ±0.64	13.67 ±1.53	21.33 ±1.63	-
Escherichia coli	1	12.5	13.4	17	18	19	19	26	-
	2	14	15	16.2	17.2	17	18	24.3	-
	3	13	14	17	17.3	16.5	17.2	25	-
	Mean	13.17±0.58	14.13±0.81	16.73 ±0.69	17.50±0.44	17.50±1.54	18.07±0.90	25.10±0.85	-

Note: +Ve = positive controle and –ve = negative controle.

Staphylococcus aureus Salmonella

Escherichia coli

Figure 26: Antibacterial activity of Fe_2O_3 nanoparticles synthesized using *Adhatoda schimperiana* aqueous leaf extract.

5. Conclusion and Recommendations

5.1 Conclusion

The current study developed an eco-friendly approach for synthesizing Fe_2O_3 nanoparticles utilizing *Adhatoda schimperiana* aqueous leaf extract. The phytochemical screening results confirmed the presence of phenols, saponins, alkaloids, and flavonoids in leaf extracts. UV-Vis, TGA, FT-IR, XRD, and BET methods were used to characterize the Fe_2O_3 nanoparticle, verifying its successful production. The UV-Vis absorbance peak (λ_{max}=397 nm) provided information on the crystallite size of the Fe_2O_3 nanoparticle. The results showed that the band gap of Fe_2O_3 nanoparticles was 2.18 eV, which is pretty good compared to other green synthesis methods. The presence of major functional groups was identified from the FT-IR spectra, and its absorbance peak was lowered to 574.1 cm^{-1} and 443.3 cm^{-1}, indicating the synthesis of Fe_2O_3 nanoparticles. This was confirmed the existence of active chemicals in the extract, which may greatly contribute to nanoparticle stabilization, as previously described. Furthermore, the XRD results revealed that the average crsthyline size of the synthesized Fe_2O_3 nanoparticles produced using the green synthesis approach was 14.31 nm. It was in good agreement with the reported value and with standard data card (JCPDS No: 033-0664) The TGA revealed three mass losses and the stability of Fe_2O_3 nanoparticles, while DTA produced three endothermic peaks at different temperatures. The curve becomes parallel to the temperature axis after 660 °C, high lighting the great stability of IONPs. The BET surface area of uncalicinated and calcined Fe_2O_3 nanoparticles was determined as 276.325 m^2/g and 286.861 m^2/g. The pore volume of Fe_2O_3 nanoparticles was measured to be 5.46 cc/g and 4.57 cc/g respectively which is excellent surface area to compared with other literature. The photo catalytic degradation of Fe_2O_3 nanoparticle was investigated using methylene blue dye in the presence of visible light, and the results ensured a drastic improvement from the earlier reports of the photo catalytic activity of Fe_2O_3 nanoparticle and *Adhatoda schimperiana* leaf extract-derived Fe_2O_3 nanoparticle showed the maximum zone of inhibition was observed against *Salmonella* (13.7 mm), followed by *Escherichia coli* (18 mm) and *Staphylococcus aureus* (16 mm) at 100 μg/l concentrations .As a result, the designed plant leaf-mediated Fe_2O_3 nanoparticle synthesis has provided avenues for the enhancement of high-efficiency photo catalytic degradation and antibacterial activity due to the small size and high surface area of Fe_2O_3 nanoparticles, allowing the desired objectives to be fruitfully attained.

5.2 Recommendations

From this study, the following recommendation has been forwarded:

- ✓ SEM, TEM, and EDX techniques are used to further characterize the surface morphology, composition, stability, moisture content, and form of the produced Fe_2O_3 nanoparticles.
- ✓ Further research is needed to determine the effectiveness of plant extract-mediated Fe_2O_3 nanoparticles for photo catalytic degradation of various organic dyes.
- ✓ It is also recommended that the synthesized Fe_2O_3 nanoparticle needs additional study for more applications like sensor and antioxidant activity.
- ✓ The synthesized Fe_2O_3 nanoparticle was showing the excellent surface area, energy band gap, average crystalline size and stability, so this nanoparticle could be used for degradation methyl blue and antibacterial activity application.

6. References

1. Ogidi, O.I. and U.M. Akpan, *Aquatic biodiversity loss: impacts of pollution and anthropogenic activities and strategies for conservation*, in *Biodiversity in Africa: potentials, threats and conservation*. 2022:p. 421-448.

2. Islam, M.T., *et al.*, *Synthetic dyes for textile colouration: process, factors and environmental impact.* 2022: p. 327-373.

3. Dutta, S., *et al.*, *Contamination of textile dyes in aquatic environment: Adverse impacts on aquatic ecosystem and human health, and its management using bioremediation.* 2024: p. 120103.

4. Nair, G.M., T. Sajini, and B.J.T.O. Mathew, *Advanced green approaches for metal and metal oxide nanoparticles synthesis and their environmental applications.* 2022: p. 1080.

5. Dolai, J., K. Mandal, and N.R.J.A.A.N.M. Jana, *Nanoparticle size effects in biomedical applications.* 2021: p. 6471-6496.

6. Jeevanandam, J., *et al.*, *Green approaches for the synthesis of metal and metal oxide nanoparticles using microbial and plant extracts.* Nanoscale, 2022: p. 2534-2571.

7. Qamar, S.U.R. and J.N. Ahmad, *Nanoparticles: Mechanism of biosynthesis using plant extracts, bacteria, fungi, and their applications.* Journal of Molecular Liquids, 2021: p. 11640.

8. Nagar, A. and T. Pradeep, *Clean water through nanotechnology: Needs, gaps, and fulfillment.* ACS nano, 2020: p. 6420-6435.

9. Dolai, J., K. Mandal, and N.R. Jana, *Nanoparticle size effects in biomedical applications.* ACS Applied Nano Materials, 2021: p. 6471-6496.

10. Ali, Z., *et al.*, *Colorimetric sensing of heavy metals on metal doped metal oxide nanocomposites: A review.* 2023: p.187.

11. Singh, P., *et al., Biological synthesis of nanoparticles from plants and microorganisms.* Trends in biotechnology, 2016: p. 588-599.

12. Kalimuthu, K., *et al., Eco-friendly synthesis and biomedical applications of gold nanoparticles: A review.* Microchemical Journal, 2020: p. 104-296.

13. Aragaw, T.A., F.M. Bogale, and B.A. Aragaw, *Iron-based nanoparticles in wastewater treatment: A review on synthesis methods, applications, and removal mechanisms.* Journal of Saudi Chemical Society, 2021: p. 101-280.

14. Al-Hilifi, S.A., *et al., Physicochemical, morphological, and functional characterization of edible anthocyanin-enriched Aloe vera coatings on fresh figs (Ficus carica L.).* Gels, 2022: p. 645.

15. Kaur, S., S. Gupta, and P.B. Gautam, *Phytochemical analysis of Eucalyptus leaves extract.* Journal of Pharmacognosy and Phytochemistry, 2019: p. 2442-2446.

16. Usha, V., *et al., Green synthesis and characterization of antibacterial studies by iron oxide nanoparticles using Carica papaya leaf extract.* Journal of Applied Sciences and Environmental Management, 2022: p. 421-427.

17. Saeed, M., *et al., Lagenaria siceraria fruit: A review of its phytochemistry, pharmacology, and promising traditional uses.* Frontiers in Nutrition, 2022: p. 9273.

18. Zaidi, S.K., *et al., Antioxidant potential of Solanum nigrum aqueous leaves extract in modulating restraint stress-induced changes in rat's liver.* Journal of pharmacy & bioallied sciences, 2019: p. 60.

19. Poerwanto, M.E. and C. Solichah. *Potency of Guava Shoot Extract as a Control Means Against Diaphorina Citri*. in *IOP Conference Series: Earth and Environmental Science*. 2022.

20. Hooda, R. and M. Sharma, *Green synthesis, characterization and antibacterial activity of iron oxide nanoparticles.* Plant Arch, 2020: p. 1196-1200.

21. Wei, J.-N., *et al*., *Phytochemical and bioactive profile of Coriandrum sativum L.* 2019: p. 260-267.

22. Melkamu, W.W. and E.G. Feleke, *Green synthesis of copper oxide nanoparticles using leaf extract of Justicia Schimperiana and their antibacterial activity.* 2022.

23. Emebet, T., *Ethnobotanical Study of Traditional Medicinal Plants Used To Treat Human and Animal Diseases and Antibacterial Activity of Some Plants at Telemt District, North Gondar Zone of Amhara Region, Ethiopia*. 2024.

24. Al-Tohamy, R., *et al*., *A critical review on the treatment of dye-containing wastewater: Ecotoxicological and health concerns of textile dyes and possible remediation approaches for environmental safety.* 2022: p. 113-160.

25. Zhang, Z., *et al*., *Environmental impacts of hazardous waste, and management strategies to reconcile circular economy and eco-sustainability.* 2022: p. 150-856.

26. Kerr, C., *et al*., *Combination cisplatin and sulforaphane treatment reduces proliferation, invasion, and tumor formation in epidermal squamous cell carcinoma.* Molecular Carcinogenesis, 2018: p. 3-11.

27. Devi, D., *et al*., *Eco-friendly green synthesis approach and evaluation of environmental and biological applications of Iron oxide nanoparticles.* Inorganic Chemistry Communications, 2023: p. 110-700.

28. Mughal, B., *et al*., *Biogenic nanoparticles: Synthesis, characterisation and applications.* 2021: p. 2598.

29. Sethy, N.K., *et al., Green synthesis of TiO_2 nanoparticles from Syzygium cumini extract for photo-catalytic removal of lead (Pb) in explosive industrial wastewater.* Green Processing and Synthesis, 2020: p. 171-181.

30. Thakur, P. and A. Thakur, *Nanomaterials, their types and properties*, in *Synthesis and Applications of Nanoparticles*. 2022: p. 19-44.

31. Parameswaran, A.K., *et al*., *Recent progress of nanotechnology in the research framework of all-solid-state batteries.* Nano Energy, 2023: p. 107-994.

32. Pandey, P., *Role of nanotechnology in electronics: A review of recent developments and patents.* Recent Patents on Nanotechnology, 2022: p. 45-66.

33. Zhou, X.-Q., *et al*., *Zinc oxide nanoparticles: synthesis, characterization, modification, and applications in food and agriculture.* 2023: p. 1193.

34. Kumar, N. and S. Kumbhat, *Concise Concepts of Nanoscience and Nanomaterials*. 2018.

35. Adfar, Q., M. Aslam, and S.S. Maktedar, *A Compendium of Metallic Inorganic Fillers' Properties and Applications Employed in Polymers*, in *Nanofillers*. 2023:p. 25-68.

36. Chen, K., *et al*., *Insights into nucleic acid-based self-assembling nanocarriers for targeted drug delivery and controlled drug release.* 2022: p. 869-891.

37. Fatima, S., *et al.*, *Role and Perspective of Metal-Oxide Based Nanocomposites for Wastewater Treatment: A Review.* 2024: p. 128-155.

38. Shivakumar, S., A. Sharan, and K. Sadashivappa, *Experimental investigations on vibration properties of aluminium matrix composites reinforced with iron oxide particles.* Applied Mechanics and Materials, 2019: p. 122-126.

39. Digiacomo, F., *Mobility and Reactivity of Sulfate Green Rust and Sulfidized Nanoscale Zerovalent Iron for In-Situ Remediation of Chromium Contaminated Sites*. 2021.

40. Abid, N., *et al*., *Synthesis of nanomaterials using various top-down and bottom-up approaches, influencing factors, advantages, and disadvantages: A review.* 2022: p. 102-597.

41. Wagle, P.G., S.S. Tamboli, and A.P. More, *Peelable coatings: A review.* Progress in Organic Coatings, 2021: p. 106.

42. Abid, N., *et al*., *Synthesis of nanomaterials using various top-down and bottom-up approaches, influencing factors, advantages, and disadvantages: A review.* Advances in Colloid and Interface Science, 2022: p. 102-597.

43. Chen, F., *et al*., *Synthesis of nanomaterials using top-down methods.* 2022: p. 37-60.

44. Harish, V., *et al*., *Cutting-edge advances in tailoring size, shape, and functionality of nanoparticles and nanostructures: A review.* 2023: p. 1050.

45. Sorbiun, M., *et al*., *Green synthesis of zinc oxide and copper oxide nanoparticles using aqueous extract of oak fruit hull (jaft) and comparing their photocatalytic degradation of basic violet 3.* International Journal of Environmental Research, 2018: p. 29-37.

46. Jamkhande, P.G., *et al., Metal nanoparticles synthesis: An overview on methods of preparation, advantages and disadvantages, and applications.* Journal of drug delivery science and technology, 2019: p. 101-174.

47. Kim, D.-Y., *et al*., *Bioinspired silver nanoparticle-based nanocomposites for effective control of plant pathogens: A review.* Science of The Total Environment, 2023: p. 168-318.

48. Zúñiga-Miranda, J., *et al*., *Iron oxide nanoparticles: green synthesis and their antimicrobial activity.* Nanomaterials, 2023: p. 2919.

49. Singh, J., *et al., 'Green'synthesis of metals and their oxide nanoparticles: applications for environmental remediation.* Journal of nanobiotechnology, 2018: p. 1-24.

50. Alqarni, L.S., *et al*., *Green nanotechnology: Recent research on bioresource-based nanoparticle synthesis and applications.* 2022: p. 403-999.

51. Gupta, D., *et al., Green and sustainable synthesis of nanomaterials: recent advancements and limitations.* 2023: p. 116-316.

52. Dikshit, P., *et al*., *Green synthesis of metallic nanoparticles: applications and limitations. Catalysts 2021*.

53. Makarov, V., *et al.*, *"Green" nanotechnologies: synthesis of metal nanoparticles using plants.* Acta Naturae, 2014: p. 35-44.

54. Ahmad, T., *et al.*, *A critical review on phytosynthesis of gold nanoparticles: Issues, challenges and future perspectives.* Journal of Cleaner Production, 2021: p. 127-460.

55. Miu, B.A. and A. Dinischiotu, *New Green Approaches in Nanoparticles Synthesis: An Overview.* Molecules, 2022: p. 6472.

56. Kaur, M., *et al.*, *Green synthesis of metal nanoparticles and their environmental applications.* Current Opinion in Environmental Science & Health, 2022: p. 100-390.

57. Ajinkya, N., *et al*., *Magnetic iron oxide nanoparticle (IONP) synthesis to applications: present and future.* 2020: p. 4644.

58. Vasanthakumar, A., G.G. Redhi, and R.M. Gengan, *Efficient catalytic activity of ionic liquid-supported $NiFe_2O_4$ magnetic nanoparticle doped Titanium Dioxide nano-composite.* International journal of chemical engineering and applications, 2016.

59. Adhikari, A., *et al*., *Green synthesis of iron oxide nanoparticles using Psidium guajava L. leaves extract for degradation of organic dyes and anti-microbial applications.*2022: p. 1188.

60. Ben Mbarek, W., *et al*., *Effects of the addition of Fe, Co on the azo dye degradation ability of Mn-Al mechanically alloyed powders.* Metals, 2020: p. 1578.

61. Khamees, H.A. and M.A. Abid, *Green Synthesis of IONPs for Photocatalytic Activities.* Ibn AL-Haitham Journal For Pure and Applied Sciences, 2022: p. 125-135.

62. Xu, P., *et al*., *Use of iron oxide nanomaterials in wastewater treatment: a review.* Science of the total environment, 2012: p. 1-10.

63. Matlhatse, M., *Effect of Preparation Parameters of Iron Oxide Nanoparticles on the Fenton Catalytic Activity for the degradation of dye*. 2021.

64. Tomar, S., *et al*., *Treatment of Textile-Wastewater Using Green Technologies.* Green Chemistry for Sustainable Water Purification, 2023: p. 129-156.

65. Periyasamy, A.P.J.S., *Recent advances in the remediation of textile-dye-containing wastewater: prioritizing human health and sustainable wastewater treatment.* 2024: p. 495.

66. Al-Tohamy, R., *et al*., *A critical review on the treatment of dye-containing wastewater: Ecotoxicological and health concerns of textile dyes and possible remediation approaches for environmental safety*. Ecotoxicology and Environmental Safety, 2022: p. 113-160.

67. Masresha, A., *Green Synthesis Of Zinc Zeolite-Oxide Composite Using Hagenia Abyssinicaextract For Efficient Photocatalytic Degradation Of Methylene Blue Dye*. 2021.

68. Gupta, S.A., *et al*., *Adsorption isotherm studies of Methylene blue using activated carbon of waste fruit peel as an adsorbent.* Materials Today: Proceedings, 2022: p. 1500-1508.

69. Chand, A., *et al.*, *The prodigious hydrogen bonds with sulfur and selenium in molecular assemblies, structural biology, and functional materials.* Accounts of Chemical Research, 2020: p. 1580-1592.

70. Khan, A.A. and M. Mondal, *Effective materials in the photocatalytic treatment of dyestuffs and stained wastewater*, in *Photocatalytic Degradation of Dyes*. 2021: p. 91-111.

71. Dave, S., *et al., Dyes and Pigments: Interventions and How Safe and Sustainable Are Colors of Lif*, in *Trends and Contemporary Technologies for Photocatalytic Degradation of Dyes*. 2022: p. 1-20.

72. Tripathi, S. and T. Hussain, *Water and wastewater treatment through ozone-based technologies*, in *Development in wastewater treatment research and processes*. 2022: p. 139-172.

73. Liu, H., C. Wang, and G. Wang, *Photocatalytic advanced oxidation processes for water treatment: recent advances and perspective.* Chemistry–An Asian Journal, 2020: p. 3239-3253.

74. Alsalka, Y., *et al., Iron-based photocatalytic and photoelectrocatalytic nano-structures: Facts, perspectives, and expectations.* Applied Catalysis B: Environmental, 2019: p. 1065-1095.

75. Chen, Y., *et al., Photocatalytic oxidation of SO_2 by TiO_2: Aerosol formation and the key role of gaseous reactive oxygen species.* Environmental Science & Technology, 2021: p. 9784-9793.

76. Shao, Q., H. Lin, and M. Shao, *Determining locations of conduction bands and valence bands of semiconductor nanoparticles based on their band gaps.* ACS omega, 2020: p. 10297-10300.

77. Singh, R., P. Barman, and D. Sharma, *Synthesis, structural and optical properties of Ag doped ZnO nanoparticles with enhanced photocatalytic properties by photo degradation of organic dyes.* Journal of Materials Science: Materials in Electronics, 2017: p. 5705-5717.

78. Dao, H.M., *Methylene Blue as Light and Reactive Oxygen Species Sensitive Ligand: Applicability in Hybrid Drug and Material Synthesis*. 2021.

79. Zaheer, Z., *et al., Decolorization and mineralization of methylene blue by potassium permanganate.* Journal of Molecular Liquids, 2024: p. 123-794.

80. Yadav, N., *et al., Herbal Medicine Formulation, Standardization, and Commercialization Challenges and Sustainable Strategies for Improvement*, in *Herbal Medicine Phytochemistry: Applications and Trends*. 2023: p. 1-27.

81. Izah, S.C., *et al., Historical Perspectives and Overview of the Value of Herbal Medicine*, in *Herbal Medicine Phytochemistry: Applications and Trends*. 2023. p. 1-33.

82. Eba, T.T., *Chemical Composition And Antimicrobial Activity Study Of Root Extracts Of Justicia Schimperiana.* 2017.

83. Abebe, H. and A. Haile, *Phytochemical investigation on leaf extract of Adhatoda schimperiana, Ethiopia.* Journal of Medicinal Plants, 2014.

84. Getachew, E., *Green Synthesis of CuO Nanoparticles Using Leaf Extract of Justica Schimperiana and its Antibacterial Activity*. 2020.

85. Tedila, H. and A.A.V. Shanmugam, *In-vitro antibacterial activity of Ruta chalepensis (Tenadam) and Justicia shimperiana (Senel) plants against some bacterial human pathogens.* In-Vitro, 2019.

86. Ahmad, A., *et al*., *Benign-by-design plant extract-mediated preparation of copper oxide nanoparticles for environmentally related applications.* Environmental Research, 2024: p. 1180.

87. Tola, M.A., *et al., Traditional Herbal Remedies in the Management of Metabolic Disorders in Ethiopia: A Systematic Review of Ethnobotanical Studies and Pharmacological Activities.* Evidence-Based Complementary and Alternative Medicine, 2023.

88. Gizaw, A., *et al., Phytochemical screening and in vitrolousicidal and acaricidal activities of Justicia schimperiana (Hochst. ex Nees) T. Anderson leaf in West Showa Zone, Ethiopia.* Annals of Phytomedicine, 2022: p. 725-731.

89. Seifu, A., *Bioprospecting potential of Justicia schimperiana for Access and Benefit Sharing.* 2017.

90. Khan, S., *et al., Biosynthesis and characterization of iron oxide nanoparticles from Mentha spicata and screening its combating potential against Phytophthora infestans.* Frontiers in Plant Science, 2022**:** p. 100-1499.

91. Pillai, M., M. Mpopo, and M. SB, *Phytochemical analysis, total phenolic, total flavonoid contents and ferric reducing power of extracts from roots and leaves of Searsia burchellii.*2021.

92. Abhaykumar, K., *Phytochemical studies on Achyranthes aspera.* World Scientific News, 2018: p. 16-34.

93. Abhaykumar, K.J.W.S.N., *Phytochemical studies on Achyranthes aspera.* 2018: p. 16-34.

94. Maheshwaran, L., *et al*., *Phytochemical Testing Methodologies and Principles for Preliminary Screening/Qualitative Testing.* 2024: p. 11-38.

95. Oludare, T., *Qualitative and Quantitative Screening of Phytochemical Analysis of Spondiasmombin (Linn.) Extracts (Root, Leaf, and Stem Bark), A Useful Formulation in Drug Discovery.* SF J Anal Biochem, 2018.

96. Shaikh, J.R. and M. Patil, *Qualitative tests for preliminary phytochemical screening: An overview.* International Journal of Chemical Studies, 2020: p. 603-608.

97. Ali, A., *et al.*, *Synthesis, characterization, applications, and challenges of iron oxide nanoparticles.* Nanotechnology, science and applications, 2016: p. 49-67.

98. Škugor, B. and J. Deur, *A novel model of electric vehicle fleet aggregate battery for energy planning studies.* Energy, 2015: p. 444-455.

99. Loganathan, S., *et al.*, *Thermogravimetric analysis for characterization of nanomaterials*, in *Thermal and rheological measurement techniques for nanomaterials characterization*. 2017: p. 67-108.

100. Sathiyavimal, S., *et al*., *Green synthesis of copper oxide nanoparticles using Abutilon indicum leaves extract and their evaluation of antibacterial, anticancer in human A549 lung and MDA-MB-231 breast cancer cells.* Food and Chemical Toxicology, 2022: p. 113-330.

101. Dawra, M.B.A., *Determination of Some Optical and Electrical Properties for Fe Oxide Doped by Al and Cu Using X-Ray Diffraction and Ultra Violet Spectrometer*. 2023.

102. Mpelane, S., *et al.*, *Synthesis of mesoporous iron oxide nanoparticles for adsorptive removal of levofloxacin from aqueous solutions: Kinetics, isotherms, thermodynamics and mechanism.* 2022: p. 8457-8468.

103. Alene, A.N., *et al*., *Utilization of a novel low-cost Gibto (Lupinus Albus) seed peel waste for the removal of malachite green dye: equilibrium, kinetic, and thermodynamic studies.* Journal of Chemistry, 2021: p. 1-16.

104. Zare, M., *et al.*, *Novel green biomimetic approach for synthesis of ZnO-Ag nanocomposite; antimicrobial activity against food-borne pathogen, biocompatibility and solar photocatalysis.* Scientific reports, 2019: p. 8303.

105. Saeed, M., *et al*., *Azadirachta indica leaves extract assisted green synthesis of Ag-TiO_2 for degradation of Methylene blue and Rhodamine B dyes in aqueous medium.* Green Processing and Synthesis, 2019: p. 659-666.

106. Abou-Dobara, M.I., *et al.*, *Antibacterial activity of extracellular biosynthesized iron oxide nanoparticles against locally isolated β-lactamase-producing Escherichia coli from Egypt.* 2024: p. 113.

107. Tawhid, T., *Comprehensive study of antibacterial activities of medicinal plants and essential oils against Staphylococcus aureus*. 2021.

108. Mengistu, N., *Proximate Analysis, and Determination of Mineral Composition, Phytochemical Contents, Antioxidant and Antibacterial Activities of Methanol Extracts of Portulaca Qurdifirda L*. 2023.

109. Esfanddarani, H.M. and M.J.J.o.M.S. Panigrahi, *Phytosynthesis of transition (Ni, Fe, Co, Cr, and Mn) metals and their oxide nanoparticles for biomedical applications: a review.* 2024: p. 1-47.

110. Kem, A., *et al., Eco-friendly green synthesis of stable ZnO nanoparticles using citrus limon: X-ray diffraction analysis and optical properties.* 2022: p. 85-814.

111. Supin, K., P.N. PM, and M.J.R.a. Vasundhara, *Enhanced photocatalytic activity in ZnO nanoparticles developed using novel Lepidagathis ananthapuramensis leaf extract.* 2023: p. 1497-1515.

112. Mohamed, A., *et al*., *Green synthesis and characterization of iron oxide nanoparticles for the removal of heavy metals (Cd^{2+} and Ni^{2+}) from aqueous solutions with Antimicrobial Investigation.* 2023: p. 7227.

113. Gebre, S.H.J.J.o.C.S., *Bio-inspired synthesis of metal and metal oxide nanoparticles: the key role of phytochemicals.* 2023: p. 665-704.

114. Wasly, H., M.A. El-Sadek, and M.J.A.P.A. Henini, *Influence of reaction time and synthesis temperature on the physical properties of ZnO nanoparticles synthesized by the hydrothermal method.* 2018: p. 1-12.

115. Saha, N., B. Sarkar, and K.J.J.o.M.L. Sen, *Aqueous biphasic systems: A robust platform for green extraction of biomolecules.* 2022 : p. 119-882.

116. Akintelu, S.A., *et al.*, *Green synthesis of iron oxide nanoparticles for biomedical application and environmental remediation: a review.* 2021: p. 17-37.

117. Aboelfetoh, E.F., A.E. Aboubaraka, and E.-Z.M.J.J.o.C.S. Ebeid, *Synergistic effect of iron and copper oxides in the removal of organic dyes through thermal induced catalytic degradation process.* 2023: p. 2521-2535.

118. Ibrahim, A.M., *et al.*, *Ovicidal, immunotoxic and endocrine disrupting effects of saponin on Bulinus truncatus snails with special emphasize on the oxidative stress parameters, genotoxicological, and histopathological alterations.* 2023: p. 78641-78652.

119. Patil, R.B. and A.D.J.M.T.P. Chougale, *Analytical methods for the identification and characterization of silver nanoparticles: A brief review.* 2021: p. 5520-5532.

120. Zakariya, N.A., S. Majeed, and W.H.W.J.S.I. Jusof, *Investigation of antioxidant and antibacterial activity of iron oxide nanoparticles synthesized from the aqueous extract of Penicillium spp.* 2022: p. 100-164.

121. Andrade, P.H., *et al.*, *Band gap analysis in MOF materials: Distinguishing direct and indirect transitions using UV–vis spectroscopy.* 2024: p. 1020.

122. Kumar, P., *et al.*, *Catalyzing innovation: Exploring iron oxide nanoparticles-Origins, advancements, and future application horizons.* 2024: p. 215-750.

123. Satarzadeh, N., *et al., Purification, Characterization, and Assessment of Anticancer Activity of Iron Oxide Nanoparticles Biosynthesized by Novel Thermophilic Bacillus tequilensis Asfs1*. 2024: p. 2400.

124. Hayat, J., *et al., Phytochemical screening, polyphenols, flavonoids and tannin content, antioxidant activities and FTIR characterization of Marrubium vulgare L. from 2 different localities of Northeast of Morocco.* 2020.

125. Gupta, M., *et al*., *Effective antimicrobial activity of green ZnO nano particles of Catharanthus roseus.* 2018: p. 2030.

126. Anwar, A., *et al*., *Antimicrobial activities of green synthesized gums-stabilized nanoparticles loaded with flavonoids.* 2019: p. 3122.

127. Azizi, A., R. Norouzi Esfahani, and S.M.J.J.o.E.O.B.P. Talebi, *Essential oil analysis of Rhaponticum repens (L.) Hidalgo, and its application in green synthesis of iron nanoparticles to remove Cr (VI) ions from aqueous solutions.* 2024: p. 756-769.

128. Chandrasekar, L.B., M.D. Gnaneswari, and M.J.J.o.M.S.M.i.E. Karunakaran, *Synthesis, characterization and anti-bacterial activity of Mg and Ba-doped ZnO Nanoparticles.* 2020: p. 20270-20276.

129. Shaik, K. and S.J.P.C.R. Cole, *Comparative study of crystallite size from XRD and TEM results for pure and V_2O_5 doped CdO-$FePO_4$ composite nanopowders.* 2023: p. 241-251.

130. Rondón, B., *et al*., *Synthesis and characterization of amorphous mesoporous materials impregnated with Hematite (Fe_2O_3) for use in the H_2S removal.* 2021: p. 40-52.

131. Rao, S.M., S. Kotteeswaran, and A.M.J.I.C.C. Visagamani, *Green synthesis of zinc oxide nanoparticles from camellia sinensis: Organic dye degradation and antibacterial activity.* 2021: p. 108-956.

132. Wang, Y., *et al., Facile synthesis of porous α-Fe_2O_3 nanorods and their application in ethanol sensors.* 2008:p. 17804-17808.

133. Mwebembezi, T., *et al., Synthesis, characterization and application of steel waste-based iron oxide nanoparticles for removal of heavy metals from industrial wastewaters.* 2024.

134. Varghese, T., *et al., Co-doping of Fe_2O_3 nanoparticles with Y and Zr by green synthesis.* 2024: p. 137-383.

135. Shah, Y., *et al., Peltophorum pterocarpum leaf extract mediated green synthesis of novel iron oxide particles for application in photocatalytic and catalytic removal of organic pollutants.* 2022: p. 1-14.

136. Samrot, A.V., *et al., A review on synthesis, characterization and potential biological applications of superparamagnetic iron oxide nanoparticles.* 2021: p. 1042.

137. Kim, S.J., *et al., Morphology-Controlled Nickel Oxide and Iron–Nickel Oxide for Electrochemical Oxygen Evolution Reaction.* 2023: p. 8360-8367.

138. Etafo, N.O., *et al., Revolutionizing photocatalysis: Unveiling efficient alternatives to titanium (IV) oxide and zinc oxide for comprehensive environmental remediation.* 2024: p. 105-369.

139. Alene, A.N., *et al., Utilization of a Novel Low-Cost Gibto (Lupinus Albus) Seed Peel Waste for the Removal of Malachite Green Dye: Equilibrium, Kinetic, and Thermodynamic Studies.* 2021: p. 661-8510.

140. Khasawneh, O.F.S., *et al., Removal of acetaminophen using Fe_2O_3-TiO_2 nanocomposites by photocatalysis under simulated solar irradiation: optimization study.* 2021: p. 104-921.

141. Yang, X., *et al., Rapid degradation of methylene blue in a novel heterogeneous Fe_3O_4 and TiO_2-catalyzed photo-Fenton system.* 2015.p. 106.

142. Abdulkadir, B.A., *et al., Synergistic effects of Fe_2O_3 supported on dendritic fibrous SBA-15 for superior photocatalytic degradation of methylene blue.* 2025: p. 108-859.

143. Saeed, M., *et al., Azadirachta indica leaves extract assisted green synthesis of Ag-TiO_2 for degradation of Methylene blue and Rhodamine B dyes in aqueous medium.* 2019: p. 659-666.

144. Shi, W., *et al., Dual enhancement of capturing photogenerated electrons by loading CoP nanoparticles on N-deficient graphitic carbon nitride for efficient photocatalytic degradation of tetracycline under visible light.* 2020: p. 116-930.

145. Harandi, F.N., *et al., Surface modification of electrospun wound dressing material by Fe_2O_3 nanoparticles incorporating Lactobacillus strains for enhanced antimicrobial and antibiofilm activity.* 2022: p. 101-592.

146. Kadhim, D.A., *et al., Development of iron oxide nanoparticles using egg peel (brown) extract as a useful tool for removing the MB dye.* 2024: p. 117.

7. Appendix

(Appendix A) the effect of precursor concentration.

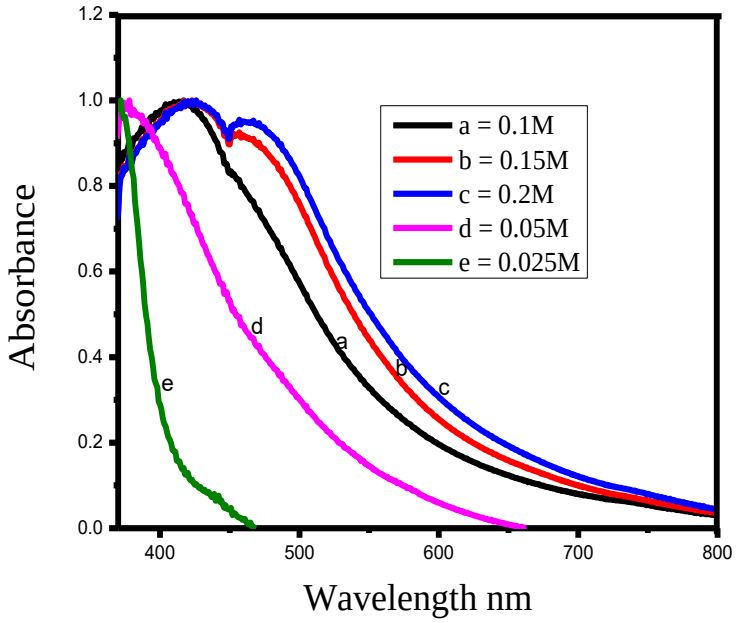

Figure 27: The effect of precursor concentration.

(Appendix B) Varying volumes ratio of precursor and extract.

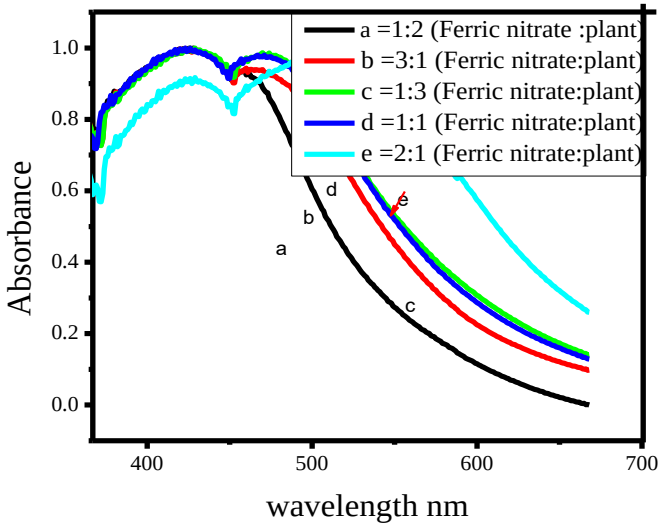

Figure 28: Varying volumes ratio of precursor and extract.

(Appendix C) The effect of varying reaction time.

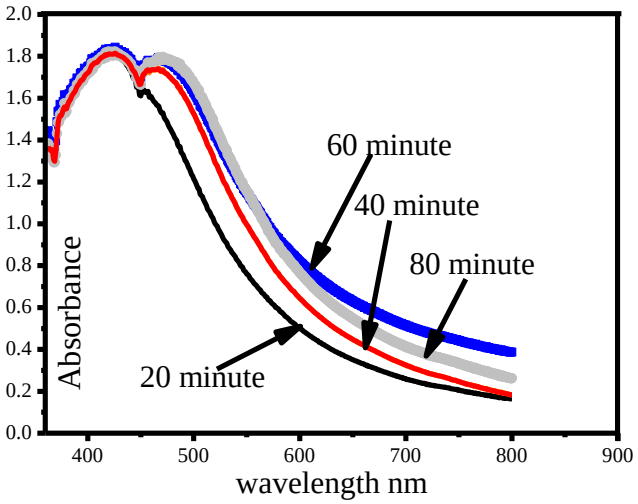

Figure 29: The effect of varying reaction time.

(Appendix D) the effect of pH on IONPs synthesis.

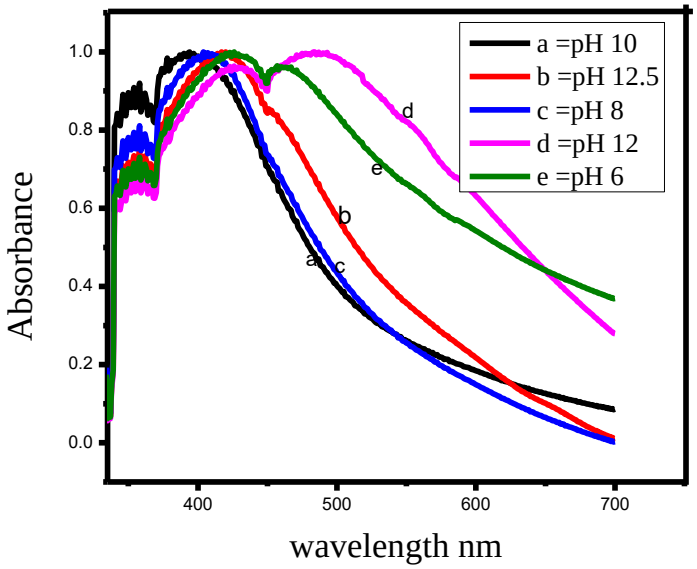

Figure 30: The effect of pH on IONPs synthesis.

(Appendix E) the effect of temperature on IOPs synthesis

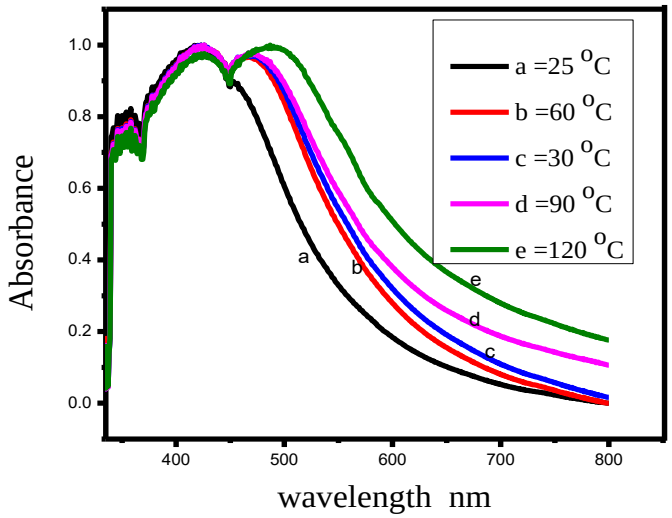

Figure 31: The effect of temperature on IONPs synthesis.

(Appendix F) the effect of plant extract on IONPs synthesis.

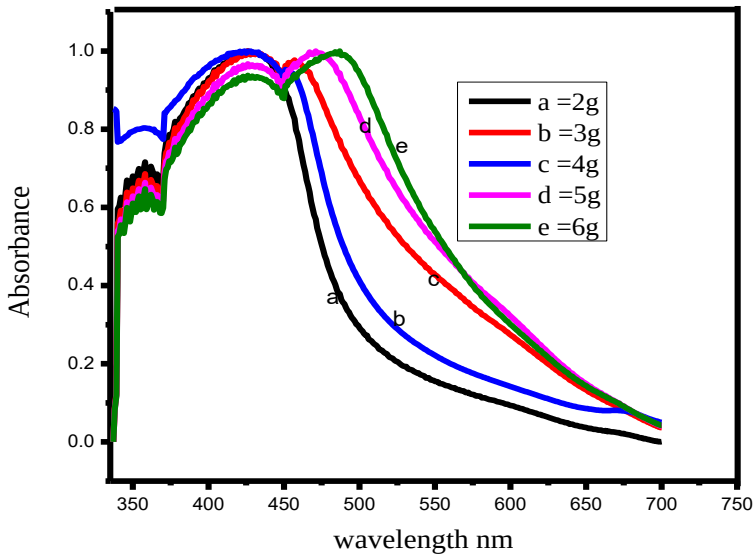

Figure 32: The effect of plant extract on IONPs synthesis.

Appendix G

Table 5: The optimization of parameters and their optimal value.

No	Optimize parameters	Concentration range	The other parameters values used during test.	Optimal value
1	Precursor(Ferric nitrate)	(0.025,0.05,0.1and 0.2) M	pH10, 3% w/v plant powder, 60 min, 80 ^{o}C, and 1:2 ratio of ferric nitrate to plant extract.	0.1 M
2	Volumes ratio of precursor and plant extract	(1:1, 2:1, 1:2, 3:1,and 1:3) mL	0.1M, pH10, 60 min, 80 ^{o}C and 3% w/v.	1:2 v/v
3	Reaction time	20 to 90 minutes	0.1 M, 1:2 v/v, pH=10 ,80 ^{o}C and 3% w/v,	60 minute
4	pH	6-12	0.1 M, 3% w/v, 60 min, 80 ^{o}C and 1:2 v/v,	10
5	Temperature	25 ^{o}C to 120 ^{o}C	0.1 M, pH10,3% w/v,1:2 v/v and 60 min.	60 ^{o}C
6	Plant extract powder	2 to 6 g	0.1 M, pH10, 1:2 v/v, 60 minute and 60 ^{o}C.	2 g(2% w/v)

Appendix H

Table 6: Percent degradation of both catalyzed with IONPs and uncatalyzed MB dyes.

Time (min)	λmax (nm)	MB (Catalyzed with IONPs		MB (Uncatalyzed)	
		Absorbance	%D	Absorbance	%D
0	664	1.431665	-------	1.451	------
20	664	0.822993	42.515	1.383	4.686
40	664	0.627135	56.195	1.361	6.203
60	664	0.363795	74.589	1.352	6.818
80	664	0.240382	83.210	1.343	7.443
100	664	0.093954	93.437	1.270	12.474

120	664	0.041776	**97.082**	1.250	13.852
140	664	0.041862	97.076	1.214	16.333
160	664	----------	----------	1.188	18.125
180	664	----------	----------	1.143	21.227
200	664	----------	----------	1.082	**25.431**

- **Decolorization of MB dye catalyzed by Fe_2O_3 NPs.**

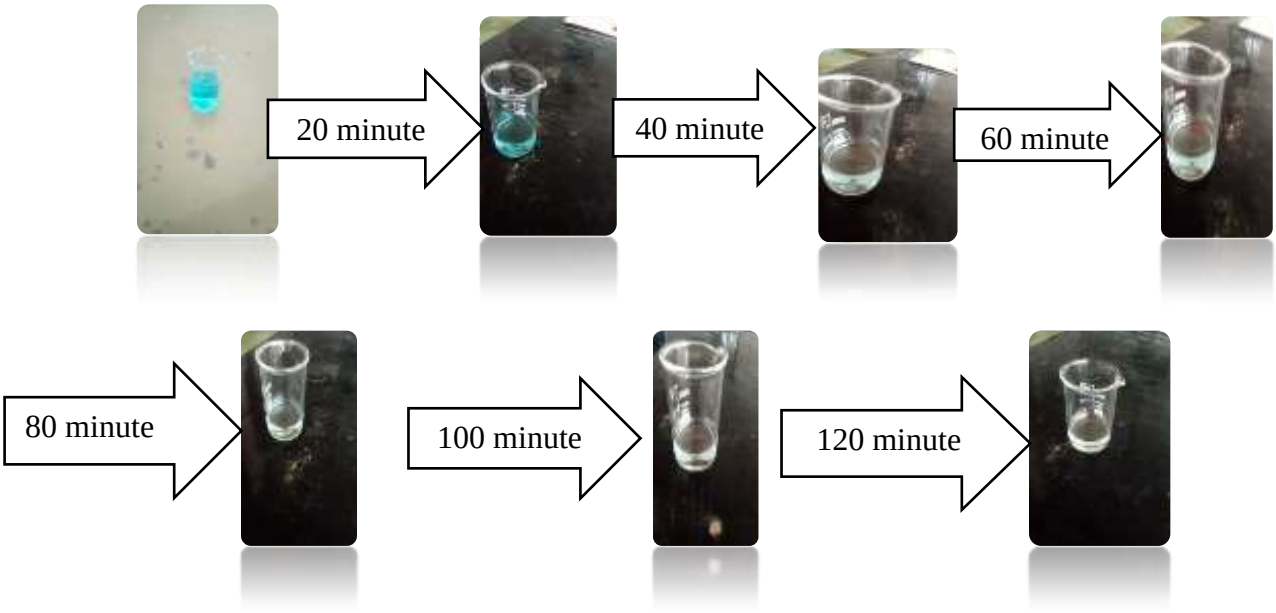

- **Decolorization of MB dye catalyzed by natural sunlight.**

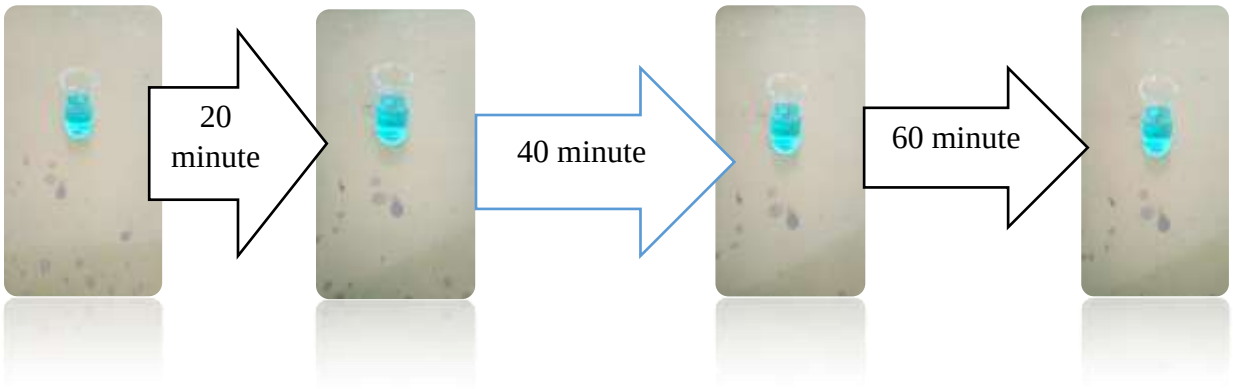

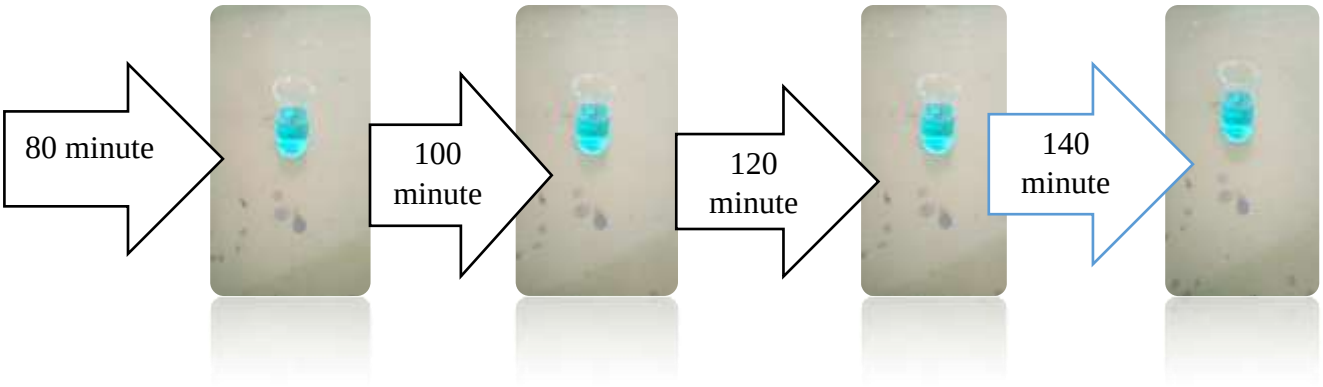
80 minute
100 minute
120 minute
140 minute